serum vitamin concentrations with Hcy and BMD among subjects in the same study.

In the present study, to evaluate nutritional risk factors for osteoporosis in patients with type 2 diabetes, BMD, Hcy level, and intakes and levels of Hcy-related vitamins including folate, vitamin B_6 and vitamin B_{12} were analyzed.

MATERIALS AND METHODS

Study Population

A total of 125 Japanese patients with type 2 diabetes admitted between December 2008 and June 2009 to Kyoto University Hospital were sequentially enrolled in the study. Lateral lumbar X-ray was carried out to exclude those with scoliosis, compression fractures and ectopic calcifications. Subjects with bilateral hip fractures or prosthesis and other diseases that might influence bone metabolism including liver disease, renal dysfunction (serum creatinine above 2 mg/dL), hyperthyroidism, hyperparathyroidism, hypercorticoidism, and hypogonadism were excluded. All subjects were free of drugs that influence bone and calcium metabolism including glucocorticoids, bisphosphonates, calcitonin injection, estrogens, selective estrogen receptor modulators, vitamin D, vitamin K, thiazide diuretics, heparin and anticonvulsants. The number of patients treated with thiazolidinedione and metformin was 7 and 28, respectively. The present study was cross-sectional in design, and was approved by The Ethical Committee of Kyoto University Hospital and complies with the Helsinki Declaration. Written informed consent was obtained from all participants.

Measurement of Bone Mineral Density

BMD was measured by dual-energy X-ray absorptiometry (DXA; Discovery; Hologic, Waltham, MA, USA) at the lumbar spine (L1-L4) and femoral neck. The coefficient of variation of the measurements of BMD was 0.39%. BMD (g/cm^2) was expressed as *Z*-score calculated on the basis of the normal reference values of the age- and sex-matched Japanese group provided by the DXA system manufacturer. Because male and female patients of different ages were included in the study, comparison of BMD was made based on *Z*-scores. Fat mass and lean body mass (without bone mineral content) were measured by DXA (Hologic Discovery; Hologic) using whole-body absorptiometry software, and each value was expressed in kilograms.

Biochemical Measurements

Blood samples were obtained after overnight fasting immediately after admission. Glycosylated hemoglobin (HbA_{1c}) was measured by high performance liquid chromatography (HPLC). The value for HbA_{1c} (%) is estimated as a National Glycohemoglobin Standardization Program (NGSP) equivalent value (%) calculated by the formula HbA_{1c} (%) = HbA_{1c} [Japan Diabetes Society (JDS); %] +0.4%, considering the relational expression of HbA_{1c} (JDS; %) measured by the previous Japanese standard substance and measurement methods and HbA_{1c} (NGSP)[22]. Fasting serum C-peptide was measured by ELISA (ST AIA-PACK C-Peptide; Toso Corporation, Tokyo, Japan). Bone-specific alkaline phosphatase (BAP) was measured by enzyme immunoassay (Osteolinks BAP; DS Pharma Biomedical, Suita, Japan), and urine N-terminal cross-linked telopeptide of type-I collagen (uNTx) was measured by ELISA (Osteomark NTx ELISA Urine; Inverness Medical, Waltham, MA, USA). Plasma Hcy levels were determined by HPLC using a thiol-specific fluorogenic reagent, ammonium 7-fluorobenzo-2-oxa-1,3-diazole-4-sulfate[23], and the upper limit of Hcy was 13.5 nmol/L. As pyridoxal 5′-phosphate (PLP) is the predominant circulating form of vitamin B_6, serum PLP concentrations were measured by HPLC[24,25] for evaluation of vitamin B_6 status. For vitamin B_{12} measurement, 0.2 mmol/L acetate buffer (pH 4.8) was added to the serum samples, and the vitamin B_{12} was converted to cyanocobalamin by boiling with 0.0006% potassium cyanide at acidic pH. Cyanocobalamin was determined by the microbioassay method using *Lactobacillus leichmanii*, ATCC 7830[24,25]. Serum folate was determined by the microbioassay method using *Lactobacillus casei* ATCC 2733[24,25].

Evaluation of Dietary Nutrient Intake

A food frequency questionnaire (FFQ) validated by Takahashi *et al.*[26,27] was used to calculate nutrient intakes. The FFQ used in the present study included questions on the consumption of various food items over the previous 1 or 2 months. Daily nutrient intake was calculated by multiplying the frequency of consumption of each food by the nutrient content of the portion size and summing the products for all food items. The FFQ is validated against 7-day dietary records and the FFQ-estimated nutrient intake values are 72–121% of those of 7-day dietary records[26]. The reproducibility of the FFQ at intervals of 1–2 months is 93–119% for each nutrient[26]. Correlations of dietary folate intake, serum folate concentration, and plasma Hcy level with intakes of various food groups including grain/rice, potato, green vegetables, other vegetables, fruits, seaweeds, beans/soy products, seafood, meats, egg, milk products and oil/fat were evaluated.

Statistical Analysis

Data were expressed as mean ± SD. SPSS statistical software (version 13.0; SPSS, Chicago, IL, USA) was used for all statistical analyses. Pearson's correlation coefficient was calculated as a measure of association by adjusting for age and sex where appropriate. Stepwise multiple linear regression analyses were carried out to determine independent factors for plasma Hcy levels including (i) dietary vitamin B_6, vitamin B_{12} and folate intake values; and (ii) serum PLP, vitamin B_{12} and folate concentrations as independent variables. The relationship between BMD with Hcy and Hcy-related vitamins was further explored using a quartile-based analysis. Statistical differences among the groups were evaluated using analysis of covariance (ANCOVA) adjusted for age and sex, and Dunnett's multiple comparison tests by comparison with the highest Hcy group. $P < 0.05$ was considered significant.

RESULTS

Clinical characteristics, laboratory data and nutrient intake of subjects are shown in Table 1. The average serum vitamin B_{12} concentration was 1.45 ± 0.45 pmol/mL (Table 1) and there was no difference between patients taking metformin (1.52 ± 0.49 pmol/mL, $n = 97$) and those without (1.43 ± 0.49 pmol/mL, $n = 28$). Nutrient intake values were significantly positively correlated with total energy intake (Table 2). Dietary vitamin B_6, vitamin B_{12} and folate intake values were positively correlated with serum vitamin B_6, vitamin B_{12} and folate levels, respectively (Table 2). Plasma Hcy levels were negatively correlated with both dietary intake and serum concentration of folate (Table 2). Only vitamin B_6 intake and not vitamin B_6 concentration showed a weak negative correlation with Hcy; the influence of vitamin B_{12} on Hcy elevation was unclear (Table 2). Stepwise multiple linear regression analyses were carried out to determine independent factors for plasma Hcy levels. Dietary folate intake was a significant predictor of Hcy when dietary vitamin B_6, vitamin B_{12} and folate intake values were included as independent variables ($R^2 = 0.088$, β-coefficient = −0.297, $P < 0.001$), and serum folate concentration also was a significant predictor of Hcy when serum PLP, vitamin B_{12} and folate concentrations were included as independent variables ($R^2 = 0.121$, β-coefficient = −0.347, $P < 0.001$). We then evaluated the correlations of folate intake and the concentrations of folate and Hcy with intake of the various food groups determined by FFQ. Dietary folate intake and serum folate concentration were significantly associated with intakes of certain food groups including potato, green vegetables, other vegetables and fruits. Only intake of green vegetables was significantly correlated with the plasma Hcy level (Table 3).

Bone mineral density of lumbar spine (SP-BMD) and femoral neck (FN-BMD) were positively correlated with body mass index (BMI) and fat mass, although no significant correlations were found in diabetes-related parameters including fasting plasma glucose, HbA_{1c} and diabetes duration (Table 4). Both SP-BMD and FN-BMD were positively correlated with fasting serum C-peptide, but these correlations were cancelled when adjusted for BMI. Urinary NTx, a marker of bone resorption, was negatively correlated with FN-BMD. As nutrient intake significantly increases with energy intake, nutrition intakes were also evaluated by adjusting for calories. As a result, calorie-adjusted folate intake was positively correlated with SP-BMD, although the association between calorie-adjusted folate and FN-BMD did not reach statistical significance. There were no significant associations between BMD of both sites and serum concentrations of vitamin B_6, vitamin B_{12} and folate. The plasma Hcy concentration was negatively correlated with both

Table 1 | Background characteristics of the study subjects

Characteristic	
No. subjects	125
Male/female	79 (63.2%)/46 (36.8%)
Age (years)	61.2 ± 12.4
Duration of diabetes (years)	11.2 ± 9.4
Diabetes treatment (diet/OHA/Ins/Ins + OHA)	27 (21.6%)/62 (49.6%)/28 (22.4%)/8 (6.4%)
BMI (kg/m^2)	24.9 ± 4.9
Fat mass (kg)	16.5 ± 9.8
Lean body mass (kg)	45.9 ± 9.3
Fasting plasma glucose (mg/dL)	160.2 ± 48.6
HbA_{1c} (%)	9.6 ± 2.2
Fasting serum C-peptide (ng/mL)	1.71 ± 0.89
Serum BAP (U/L)	23.5 ± 8.7
uNTx (nMBCE/mmol Cr)	35.6 ± 19.8
Energy intake (kcal/day)	2073.2 ± 582.5
Protein/fat/carbohydrate intake (g/day)	73.6 ± 19.7/64.4 ± 23.7/278.7 ± 80.2
Calcium intake (mg/day)	596.0 ± 213.6
Vitamin D intake (μg/day)	9.21 ± 4.48
Vitamin B_6 intake (mg/day)	1.22 ± 0.34
Vitamin B_{12} intake (μg/day)	8.81 ± 4.65
Folate intake (μg/day)	287.4 ± 100.5
Serum PLP concentration (pmol/mL)	61.3 ± 29.1
Serum vitamin B_{12} concentration (pmol/mL)	1.45 ± 0.45
Serum folate concentration (pmol/mL)	27.5 ± 10.3
Plasma homocysteine concentration (nmol/mL)	11.2 ± 5.1

Data are number of patients (categorized data) or mean ± SD (quantitative data).
BAP, bone-specific alkaline phosphatase; BMI, body mass index; Ins, insulin; OHA, oral hypoglycemic agents; PLP, pyridoxal 5'-phosphate; uNTX, urine N-terminal cross-linked telopeptide of type-I collagen.

Table 2 | Correlations among dietary nutrient intake values, serum concentrations and plasma homocysteine levels adjusted for age and sex

	r	P
Correlations of total energy intake with various nutrient intakes		
Vitamin B_6 (mg)	0.521	<0.001
Vitamin B_{12} (μg)	0.253	0.005
Folate (μg)	0.331	<0.001
Correlations of intake values with serum concentrations		
Vitamin B_6	0.192	0.034
Vitamin B_{12}	0.336	<0.001
Folate	0.400	<0.001
Correlations of plasma Hcy levels with B vitamins		
Vitamin B_6 intake (mg)	−0.207	0.022
Vitamin B_{12} intake (μg)	−0.001	0.988
Folate intake (μg)	−0.328	<0.001
Serum PLP concentration (pmol/mL)	0.002	0.982
Serum B_{12} concentration (pmol/mL)	0.001	0.993
Serum folate concentration (pmol/mL)	−0.369	<0.001

Hcy, homocysteine; PLP, pyridoxal 5'-phosphate.

Table 3 | Correlations of dietary folate intake, serum folate concentration and plasma homocysteine level with various food groups

	Dietary folate intake		Serum folate concentration		Plasma Hcy level	
	r	*P*	*r*	*P*	*r*	*P*
Grain/rice	−0.076	0.399	−0.086	0.341	−0.056	0.538
Potato	0.470	<0.001	0.220	0.014	0.012	0.895
Green vegetables	0.843	<0.001	0.361	<0.001	−0.207	0.020
Other vegetables	0.620	<0.001	0.197	0.027	0.077	0.390
Fruits	0.338	<0.001	0.206	0.021	0.018	0.839
Seaweeds	0.322	<0.001	0.072	0.426	0.071	0.435
Beans/soy products	0.390	<0.001	0.156	0.083	0.016	0.856
Seafood	0.313	<0.001	0.075	0.407	−0.017	0.848
Meats	0.065	0.474	0.042	0.643	−0.070	0.435
Egg	0.278	0.002	0.068	0.450	−0.056	0.538
Milk products	0.108	0.230	0.113	0.208	−0.035	0.698
Oil/fat	0.145	0.107	0.161	0.073	−0.112	0.214

Hcy, homocysteine.

Table 4 | Correlations of bone mineral density of lumbar spine and femoral neck with diabetes-related parameters, bone turnover markers and B vitamin status

	SP-BMD		FN-BMD	
	r	*P*	*r*	*P*
BMI (kg/m^2)	0.288	0.001	0.463	<0.001
Fasting plasma glucose (mg/dL)	−0.149	0.098	−0.113	0.210
HbA_{1c} (%)	0.098	0.194	0.053	0.556
Diabetes duration (years)	0.082	0.366	0.057	0.528
Fasting serum C-peptide (ng/mL)	0.182	0.045	0.285	0.001
BAP (U/L)	0.112	0.218	−0.061	0.499
uNTx (nMBCE/mmol Cr)	−0.138	0.084	−0.183	0.042
Vitamin B_6 intake (mg)	−0.032	0.727	−0.053	0.559
Vitamin B_6 intake (mg/100 kcal)	0.113	0.211	0.005	0.959
Vitamin B_{12} intake (μg)	0.012	0.899	0.166	0.065
Vitamin B_{12} intake (μg/1000 kcal)	0.054	0.554	0.148	0.102
Folate intake (μg)	0.103	0.256	0.112	0.216
Folate intake (μg/1000 kcal)	0.198	0.027	0.153	0.090
Serum PLP concentration (pmol/mL)	−0.062	0.497	−0.007	0.936
Serum B_{12} concentration (pmol/mL)	0.023	0.799	0.058	0.524
Serum folate concentration (pmol/mL)	0.104	0.248	0.114	0.205
Plasma Hcy concentration (nmol/mL)	−0.278	0.002	−0.201	0.025

BAP, bone-specific alkaline phosphatase; BMI, body mass index; FN-BMD bone mineral density of femoral neck; Hcy, homocysteine; PLP, pyridoxal 5′-phosphate; SP-BMD, bone mineral density of lumbar spine; uNTX, urine N-terminal cross-linked telopeptide of type-I collagen.

SP-BMD and FN-BMD, showing that hyperhomocysteinemia is clearly associated with low BMD in patients with type 2 diabetes (Figure 1).

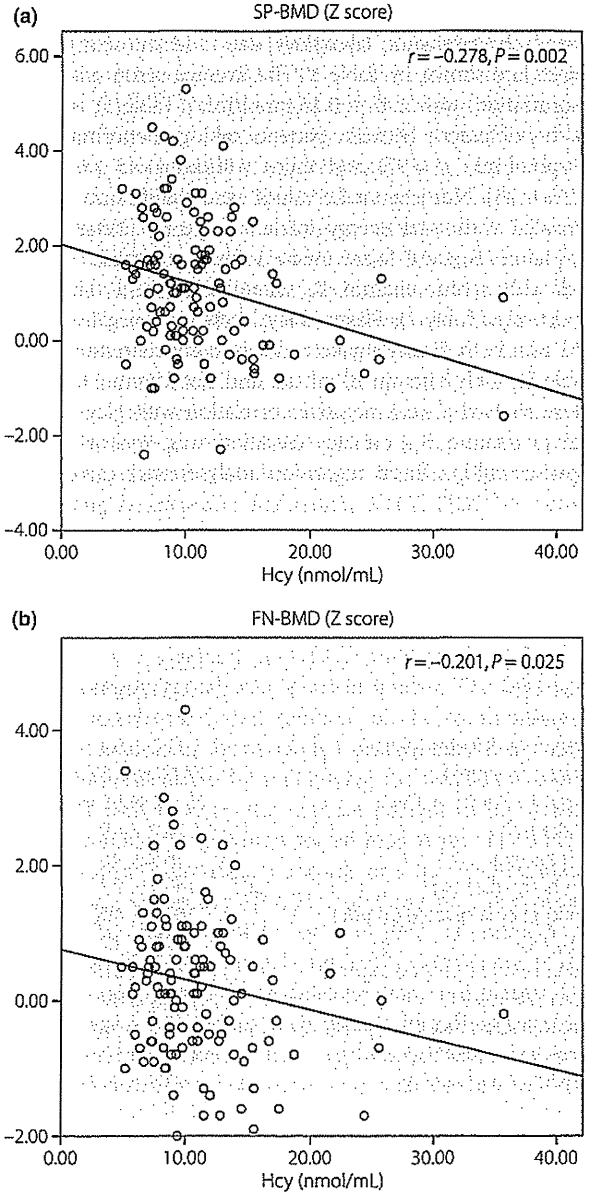

Figure 1 | The relationship between homocysteine (Hcy) and bone mineral density of lumbar spine (SP-BMD) and femoral neck (FN-BMD).

As hyperhomocysteinemia derived from folate insufficiency has been suggested to be involved in low BMD, we compared clinical characteristics of the study population across the quartiles of Hcy (quartile 1, n = 31, Hcy < 8.3 nmol/mL; quartile 2, n = 32, Hcy 8.3 to <9.9 nmol/mL; quartile 3, n = 32, Hcy 9.9 to <12.8 nmol/mL; quartile 4, n = 30, Hcy > 12.8 nmol/mL). There were no significant differences across the quartiles in general clinical characteristics including age, BMI, diabetes-related parameters, energy intake, and vitamin B_6 and vitamin B_{12} status (Table 5). However, SP-BMD and FN-BMD were significantly lower in patients in the highest quartile of Hcy than

Table 5 | Comparison of clinical characteristics according to homocysteine quartiles adjusted for age and sex

Hcy concentration (nmol/mL)	Quartile 1 (4.9–8.0)	Quartile 2 (8.1–9.9)	Quartile 3 (10.0–12.8)	Quartile 4 (12.8–35.7)	ANCOVA *P*
Male/female	17/14	21/11	23/9	18/12	
Age (years)	59.3 ± 13.8	58.1 ± 12.6	63.9 ± 8.7	64.0 ± 13.4	0.212
BMI (kg/m^2)	25.0 ± 4.4	25.8 ± 5.0	25.0 ± 5.6	23.8 ± 4.5	0.461
Fasting plasma glucose (mg/dL)	158.8 ± 44.8	162.0 ± 45.8	155.6 ± 50.0	164.6 ± 55.4	0.721
HbA_{1c} (%)	10.1 ± 2.3	9.9 ± 2.5	9.1 ± 1.8	9.4 ± 2.1	0.378
Diabetes duration (years)	9.5 ± 8.4	10.2 ± 9.7	12.6 ± 8.6	12.4 ± 9.0	0.183
SP-BMD (Z score)	1.34 ± 1.43*	1.24 ± 1.38*	1.39 ± 1.24*	0.50 ± 1.18	0.037
FN-BMD (Z score)	0.45 ± 0.99**	0.32 ± 1.23*	0.26 ± 0.96*	−0.27 ± 1.03	<0.001
Energy intake (kcal/day)	2161 ± 543	2145 ± 565	2069 ± 563	1910 ± 650	0.260
Vitamin B_6 intake (mg)	1.31 ± 0.35	1.26 ± 0.36	1.21 ± 0.32	1.09 ± 0.29	0.136
Vitamin B_{12} intake (μg)	8.59 ± 3.44	8.86 ± 4.64	9.49 ± 5.24	8.27 ± 5.21	0.798
Folate intake (μg)	323.5 ± 92.2**	287.2 ± 108.0*	305.0 ± 91.8**	231.7 ± 89.1	0.001
Intake of green vegetables (g/day)	101.9 ± 65.3*	86.1 ± 60.6	89.3 ± 47.5	68.9 ± 49.2	0.043
Serum PLP concentration (pmol/mL)	65.0 ± 33.1	60.0 ± 24.6	58.9 ± 32.9	61.4 ± 26.2	0.943
Serum B_{12} concentration (pmol/mL)	2.39 ± 0.88	2.90 ± 1.61	2.50 ± 0.73	2.53 ± 0.92	0.419
Serum folate concentration (pmol/mL)	33.6 ± 11.5**	26.9 ± 7.6*	26.9 ± 9.0*	21.7 ± 8.7	<0.001
Plasma Hcy concentration (nmol/mL)	6.9 ± 0.9**	9.1 ± 0.5**	11.3 ± 0.8**	17.8 ± 6.1	<0.001

BMI, body mass index; FN-BMD bone mineral density of femoral neck; Hcy, homocysteine; PLP, pyridoxal 5′-phosphate; SP-BMD, bone mineral density of lumbar spine. Mean ± SD, *P < 0.05, **P < 0.01 relative to the highest homocysteine quartile group.

those in patients in the other quartiles. Furthermore, patients in the highest Hcy quartile showed significantly decreased dietary folate intake, serum folate concentration and intake of green vegetables compared with those in the lower Hcy quartiles. Because the caloric intake was similar across the quartiles, the quality of the diet might be poor in the highest Hcy group. Quartile analysis revealed that the highest Hcy group showed the lowest BMD, the lowest serum folate concentration, the lowest folate intake and the lowest intake of green vegetables.

DISCUSSION

In the present study, hyperhomocysteinemia was found to be clearly associated with low BMD in type 2 diabetes patients, as it has been reported to be in non-diabetic subjects[6–14]. Furthermore, folate insufficiency might be one of the important factors in hyperhomocysteinemia, as plasma Hcy levels were negatively correlated with both dietary intake and serum concentration of folate.

Osteoporosis is a multifactorial disease, a major health problem characterized by low BMD, deterioration of bone microarchitecture and increased risk of fracture. Elevation of Hcy is one of the important risk factors for osteoporosis[28,29], and can be caused by insufficiency of Hcy-related vitamins, such as folate, vitamin B_6 and vitamin B_{12}[6–14]. Because dietary risk factors can be improved when recognized, sufficiency of Hcy-related vitamins and its relationship to osteoporosis in patients with type 2 diabetes is of primary concern.

Elevation of Hcy can be caused by insufficiency of folate, vitamin B_6 or vitamin B_{12}, and the plasma Hcy level is considered to be a fairly sensitive index of folate metabolic status compared with that of the other factors in non-diabetic subjects. Previous studies reported hyperhomocysteinemia was observed in 86% of subjects with clinically expressed folate deficiency[30]; folate is a major determinant of Hcy levels in healthy people[31,32] and vitamin B_{12} influences Hcy levels less than folate does[33,34]. Folate, vitamin B_6 and vitamin B_{12} are water-soluble vitamins, which are in general not readily stored and consistent daily intake is important. Usually, folate and vitamin B_6 deficiency develops within a month of insufficient intake. In contrast, it is known that patients with complete loss of intrinsic factor require 3–5 years to become overtly vitamin B_{12} deficient[35]. Vitamin B_{12} is a unique water-soluble vitamin, and because 80% of the 2.5 mg average whole body stock of vitamin B_{12} is reserved in the liver and vitamin B_{12} excreted in the bile and is effectively reabsorbed in the intestine, clinical signs of vitamin B_{12} deficiency take a long time to appear and progress slowly[36]. Some patients in the present study were taking metformin, which is known to inhibit absorption of vitamin B_{12}[37], but there was no difference between the patients taking metformin and those not taking metformin. As to vitamin B_6, only a weak negative correlation between vitamin B_6 intake and Hcy was not enough to conclude that vitamin B_6 is a nutritional risk factor for osteoporosis, and there have been no other studies showing the effect of vitamin B_6 on BMD.

Leafy green vegetables, such as spinach and broccoli, are rich sources of folate. Folate is also contained in a variety of foods including fruits, beans, seaweeds, liver and egg yolk. To investigate the cause of folate insufficiency, we focused particularly on dietary sources of folate. We evaluated the association of dietary folate intake, serum folate concentration, and plasma Hcy level

with various food groups, and found that intake of green vegetables correlated well with folate status and Hcy levels. Furthermore, it was revealed by the quartile analysis that the highest Hcy group showed the lowest BMD, the lowest serum folate concentration, the lowest folate intake and the lowest intake of green vegetables. This analysis suggests that insufficient intake of green vegetables, but not insufficient caloric intake, causes folate insufficiency in the group with the highest Hcy.

The strength of the present study is that it is the first study to show that nutritional status of folate might affect the homocysteine level, a putative risk factor for osteoporosis, in Japanese patients with type 2 diabetes. The present study is also meaningful in promoting awareness of the importance of diet quality, because patients with diabetes are at high risk of developing osteoporosis. In contrast, the present study has some limitations. First, the sample size was not large enough for conclusions regarding marginal insignificant *P*-values. We estimated sample size using a correlation coefficient obtained from a previous cross-sectional study assessing the relationship between BMD and plasma Hcy[8]. The correlation coefficient of femoral BMD with Hcy was −0.18 and the sample size was estimated to be $n = 153$ (two-sided $\alpha = 0.1$, $\beta = 0.2$), while we analyzed 125 patients. Second, we only analyzed patients with type 2 diabetes and comparison with non-diabetic subjects is necessary. An unanswered question is whether diabetes modulates the effects of nutritional state of folate on Hcy metabolism, and the effects of Hcy levels on BMD. Finally, a longitudinal study is required to examine the effects of Hcy on rate of BMD loss and risk of fracture for a longer duration in patients with type 2 diabetes. It is also necessary to determine whether encouraging patients with higher Hcy levels to eat more green vegetables is useful as a dietary intervention to improve Hcy levels and BMD.

In conclusion, the present study shows that BMD inversely correlates to plasma Hcy levels in Japanese patients with type 2 diabetes, and that dietary intake and the serum concentration of folate are determinant factors of Hcy levels. When our group was analyzed across quartiles, BMD, serum folate concentration, folate intake and intake of green vegetables were lowest in the highest Hcy group. Taken together, in Japanese patients with type 2 diabetes, a diet low in green vegetables rather than a calorie-restricted diet might be the more important factor in the declining nutritional status of folate that increases the Hcy level, a putative risk factor for osteoporosis.

ACKNOWLEDGEMENTS

This study was supported in part by Diabetes Masters Conference and Japan Diabetes Foundation. The authors declare no conflicts of interest.

REFERENCES

1. Vestergaard P. Discrepancies in bone mineral density and fracture risk in patients with type 1 and type 2 diabetes – a meta-analysis. *Osteoporos Int* 2007; 18: 427–444.
2. Hofbauer LC, Brueck CC, Singh SK, *et al.* Osteoporosis in patients with diabetes mellitus. *J Bone Miner Res* 2007; 22: 1317–1328.
3. Adami S. Bone health in diabetes: considerations for clinical management. *Curr Med Res Opin* 2009; 25: 1057–1072.
4. Lammes E, Törner A, Akner G. Nutrient density and variation in nutrient intake with changing energy intake in multimorbid nursing home residents. *J Hum Nutr Diet* 2009; 22: 210–218.
5. Grzybek A, Klosiewicz-Latoszek L, Targosz U. Changes in the intake of vitamins and minerals by men and women with hyperlipidemia and overweight during dietetic treatment. *Eur J Clin Nutr* 2002; 56: 1162–1168.
6. Gjesdal CG, Vollset SE, Ueland PM, *et al.* Plasma total homocysteine level and bone mineral density: the Hordaland Homocysteine Study. *Arch Intern Med* 2006; 166: 88–94.
7. Baines M, Kredan MB, Usher J, *et al.* The association of homocysteine and its determinants MTHFR genotype, folate, vitamin B_{12} and vitamin B_6 with bone mineral density in postmenopausal British women. *Bone* 2007; 40: 730–736.
8. Golbahar J, Hamidi A, Aminzadeh MA, *et al.* Association of plasma folate, plasma total homocysteine, but not methylenetetrahydrofolate reductase C667T polymorphism, with bone mineral density in postmenopausal Iranian women: a cross-sectional study. *Bone* 2004; 35: 760–765.
9. Golbahar J, Aminzadeh MA, Hamidi SA, *et al.* Association of red blood cell 5-methyltetrahydrofolate folate with bone mineral density in postmenopausal Iranian women. *Osteoporos Int* 2005; 16: 1894–1898.
10. Morris MS, Jacques PF, Selhub J. Relation between homocysteine and B-vitamin status indicators and bone mineral density in older Americans. *Bone* 2005; 37: 234–242.
11. Cagnacci A, Baldassari F, Rivolta G, *et al.* Relation of homocysteine, folate, and vitamin B_{12} to bone mineral density of postmenopausal women. *Bone* 2003; 33: 956–959.
12. Tucker KL, Hannan MT, Qiao N, *et al.* Low plasma vitamin B12 is associated with lower BMD: the Framingham Osteoporosis Study. *J Bone Miner Res* 2005; 20: 152–158.
13. Dhonukshe-Rutten RA, Pluijm SM, de Groot LC, *et al.* Homocysteine and vitamin B_{12} status relate to bone turnover markers, broadband ultrasound attenuation, and fractures in healthy elderly people. *J Bone Miner Res* 2005; 20: 921–929.
14. Dhonukshe-Rutten RA, Lips M, de Jong N, *et al.* Vitamin B-12 status is associated with bone mineral content and bone mineral density in frail elderly women but not in men. *J Nutr* 2003; 133: 801–807.
15. Harpey JP, Rosenblatt DS, Cooper BA, *et al.* Homocystinuria caused by 5,10-methylenetetrahydrofolate reductase deficiency: a case in an infant responding to methionine, folinic acid, pyridoxine, and vitamin B12 therapy. *J Pediatr* 1981; 98: 275–278.
16. Mudd SH, Skovby F, Levy HL, *et al.* The natural history of homocystinuria due to cystathionine beta-synthase deficiency. *Am J Hum Genet* 1985; 37: 1–31.

17. Lubec B, Fang-Kircher S, Lubec T, *et al.* Evidence for McKusick's hypothesis of deficient collagen cross-linking in patients with homocystinuria. *Biochim Biophys Acta* 1996; 1315: 159–162.
18. Saito M, Fujii K, Marumo K. Degree of mineralization-related collagen crosslinking in the femoral neck cancellous bone in cases of hip fracture and controls. *Calcif Tissue Int* 2006; 79: 160–168.
19. Krumdieck CL, Prince CW. Mechanisms of homocysteine toxicity on connective tissues: implications for the morbidity of aging. *J Nutr* 2000; 130: 365s–368s.
20. Koh JM, Lee YS, Kim YS, *et al.* Homocysteine enhances bone resorption by stimulation of osteoclast formation and activity through increased intracellular ROS generation. *J Bone Miner Res* 2006; 21: 1003–1011.
21. Herrmann M, Schmidt J, Umanskaya N, *et al.* Stimulation of osteoclast activity by low B-vitamin concentrations. *Bone* 2007; 41: 584–591.
22. The Committee of the Japan Diabetes Society on the Diagnostic Criteria of Diabetes Mellitus. Report of the Committee on the Classification and Diagnostic Criteria of Diabetes Mellitus. *J Diabetes Invest* 2010; 1: 212–228.
23. Araki A, Sako Y. Determination of free and total homocysteine in human plasma by high-performance liquid chromatography with fluorescence detection. *J Chromatogr* 1987; 422: 43–52.
24. Shibata K, Fukuwatari T, Watanabe T, *et al.* Intra- and inter-individual variations of blood and urinary water-soluble vitamins in Japanese young adults consuming a semi-purified diet for 7 days. *J Nutr Sci Vitaminol (Tokyo)* 2009; 55: 459–470.
25. Fukuwatari T, Yoshida E, Takahashi K, *et al.* Effect of fasting on the urinary excretion of water-soluble vitamins in humans and rats. *J Nutr Sci Vitaminol (Tokyo)* 2010; 56: 19–26.
26. Takahashi K, Yoshimura Y, Kaimoto T, *et al.* Validation of a food frequency questionnaire based on food groups for estimating indivudual nutrient intake. *Jpn J Nutr* 2001; 59: 221–232.
27. Miyaki K, Tohyama S, Murata M, *et al.* Salt intake affects the relation between hypertension and the T-786C polymorphism in the endothelial nitric oxide synthase gene. *Am J Hypertens* 2005; 18: 1556–1562.
28. van Meurs JB, Dhonukshe-Rutten RA, Pluijm SM, *et al.* Homocysteine levels and the risk of osteoporotic fracture. *N Engl J Med* 2004; 350: 2033–2041.
29. Herrmann M, Peter Schmidt J, Umanskaya N, *et al.* The role of hyperhomocysteinemia as well as folate, vitamin B_6 and B_{12} deficiencies in osteoporosis: a systematic review. *Clin Chem Lab Med* 2007; 45: 1621–1632.
30. Savage DG, Lindenbaum J, Stabler SP, *et al.* Sensitivity of serum methylmalonic acid and total homocysteine determinations for diagnosing cobalamin and folate deficiencies. *Am J Med* 1994; 96: 239–246.
31. Selhub J, Jacques PF, Wilson PW, *et al.* Vitamin status and intake as primary determinants of homocysteinemia in an elderly population. *JAMA* 1993; 270: 2693–2698.
32. Selhub J, Jacques PF, Rosenberg IH, *et al.* Serum total homocysteine concentrations in the third National Health and Nutrition Examination Survey (1991–1994): population reference ranges and contribution of vitamin status to high serum concentrations. *Ann Intern Med* 1999; 131: 331–339.
33. Lindenbaum J, Rosenberg IH, Wilson PW, *et al.* Prevalence of cobalamin deficiency in the Framingham elderly population. *Am J Clin Nutr* 1994; 60: 2–11.
34. Carmel R. *Cobalamin Deficiency, Homocysteine in Health and Disease*. Cambridge University Press, Cambridge, 2001.
35. Chanarin I. *The Megaloblastic Anemias*, 2nd edn. Blackwell Scientific, Oxford, 1979.
36. Food and Nutrition Board, Institute of Medicine. The B vitamins and choline: overview and methods. In: Institute of Medicine. *Dietary Reference Intakes: For Thiamine, Riboflavin, Niacin, Vitamin B6, Folate, Vitamin B12, Pantothenic Acid, Biotin, and Choline*. National Academy Press, Washington DC, 1998; 306–356.
37. Adams JF, Clark JS, Ireland JT, *et al.* Malabsorption of vitamin B12 and intrinsic factor secretion during biguanide therapy. *Diabetologia* 1983; 24: 16–18.

BJ www.biochemj.org

Biochem. J. (2011) 435, 421–430 (Printed in Great Britain) doi:10.1042/BJ20101708

Role of mitochondrial phosphate carrier in metabolism–secretion coupling in rat insulinoma cell line INS-1

Yuichi NISHI, Shimpei FUJIMOTO[1], Mayumi SASAKI, Eri MUKAI, Hiroki SATO, Yuichi SATO, Yumiko TAHARA, Yasuhiko NAKAMURA and Nobuya INAGAKI

Department of Diabetes and Clinical Nutrition, Graduate School of Medicine, Kyoto University, 54 Shogoin Kawahara-cho, Sakyo-ku, Kyoto 606–8507, Japan

In pancreatic β-cells, glucose-induced mitochondrial ATP production plays an important role in insulin secretion. The mitochondrial phosphate carrier PiC is a member of the SLC25 (solute carrier family 25) family and transports P_i from the cytosol into the mitochondrial matrix. Since intramitochondrial P_i is an essential substrate for mitochondrial ATP production by complex V (ATP synthase) and affects the activity of the respiratory chain, P_i transport via PiC may be a rate-limiting step for ATP production. We evaluated the role of PiC in metabolism–secretion coupling in pancreatic β-cells using INS-1 cells manipulated to reduce PiC expression by siRNA (small interfering RNA). Consequent reduction of the PiC protein level decreased glucose (10 mM)-stimulated insulin secretion, the ATP:ADP ratio in the presence of 10 mM glucose and elevation of intracellular calcium concentration in response to 10 mM glucose without affecting the mitochondrial membrane potential ($\Delta\psi_m$) in INS-1 cells. In experiments using the mitochondrial fraction of INS-1 cells in the presence of 1 mM succinate, PiC down-regulation decreased ATP production at various P_i concentrations ranging from 0.001 to 10 mM, but did not affect $\Delta\psi_m$ at 3 mM P_i. In conclusion, the P_i supply to mitochondria via PiC plays a critical role in ATP production and metabolism–secretion coupling in INS-1 cells.

Key words: inorganic phosphate (P_i), insulin secretion, mitochondria, mitochondrial phosphate carrier (PiC), small interfering RNA (siRNA), solute carrier family 25 (SLC25).

INTRODUCTION

Glucose stimulates insulin secretion by both triggering and amplifying signals in pancreatic β-cells [1]. The triggering pathway includes entry of glucose into β-cells, acceleration of glycolysis in the cytosol and mitochondrial metabolism of products derived from glycolysis, increase in ATP content and ATP/ADP ratio, closure of ATP-sensitive K^+ channels (K_{ATP} channels), membrane depolarization, opening of VDCCs (voltage-dependent Ca^{2+} channels), increase in Ca^{2+} influx through VDCCs, rise in intracellular Ca^{2+} concentration ($[Ca^{2+}]_i$), and exocytosis of insulin granules. Glucose also exerts its effects by increasing Ca^{2+} efficacy in stimulation–secretion coupling via an amplifying pathway, owing at least in part to the direct effect of increased ATP derived from glucose metabolism on exocytosis. Since depletion of mitochondrial DNA abolishes the glucose-induced ATP elevation, mitochondria are clearly a major source of ATP production in pancreatic β-cells [2,3]. Collectively, in pancreatic β-cells, intracellular glucose metabolism regulates exocytosis of insulin granules according to metabolism–secretion coupling in which glucose-induced mitochondrial ATP production plays an important role.

Almost all of the mitochondrial carrier proteins are embedded in the inner membranes of mitochondria, where they transport solutes across the membrane. They belong to the SLC25 (solute carrier family 25) group of proteins [4]. Several members of the SLC25 group have been reported to play roles in GSIS (glucose-stimulated insulin secretion) in pancreatic β-cells. Overexpression or silencing of AGC1 (aspartate/glutamate carrier 1; SLC25A12 or Aralar1) has been reported to increase or reduce GSIS in INS-1E cells respectively [5,6]. Overexpression of UCP2 (uncoupling protein 2; SLC25A8) by adenovirus vector is known to inhibit GSIS from rat islets [7], whereas GSIS from islets of UCP2-deficient mice is enhanced compared with that from control islets [8]. In addition, down-regulation of OGC (2-oxoglutarate carrier; SLC25A11), CIC (citrate/isocitrate carrier; SLC25A1) and GC1 (glutamate carrier 1; SLC25A22) by siRNA (small interfering RNA) suppress GSIS [9–11].

The mitochondrial phosphate carrier PiC (SLC25A3) is a member of the SLC25 family and transports P_i from the cytosol into the mitochondrial matrix. The *PiC* gene has 9 exons; the 3rd and the 4th exons are called exon 3A and exon 3B respectively. These two exons are alternatively spliced and two isoforms of PiC, PiC-A and PiC-B, are generated [12]. They differ considerably in their kinetic parameters as previously shown in a study using a reconstitution system [13]. The K_m of PiC-A for P_i on the external membrane surface is 3-fold that of PiC-B (PiC-A: ~2.2 mM; PiC-B: ~0.78 mM). The K_m on the internal surface is much higher (PiC-A: ~9.7 mM; PiC-B: ~6.3 mM) than K_m on the external membrane surface. The maximum transport rate of PiC-A is approximately a third that of PiC-B. These isoforms also differ in their tissue distribution. PiC-A is expressed in skeletal muscle and cardiac muscle, whereas PiC-B is expressed ubiquitously [13,14]. A case study of patients with PiC-A deficiency who suffered from lactic acidosis, heart failure and muscle weakness and died within the first year of life, demonstrates the critical significance of this carrier [15].

Since intramitochondrial P_i is an essential substrate for mitochondrial ATP production by complex V (ATP synthase) and affects activity of the respiratory chain [16], the supply of P_i from

Abbreviations used: AAC, ATP/ADP carrier; DAPP, diadenosine pentaphosphate; DIC, dicarboxylate carrier; FCCP, carbonyl cyanide *p*-trifluoromethoxyphenylhydrazone; GSIS, glucose-stimulated insulin secretion; KRBH, Krebs-Ringer bicarbonate Hepes buffer; RT, reverse transcription; siRNA, small interfering RNA; SLC25, solute carrier family 25; TMPD, *N*,*N*,*N*′,*N*′-tetramethyl-*p*-phenylenediamine.

[1] To whom correspondence should be addressed (email fujimoto@metab.kuhp.kyoto-u.ac.jp).

cytosol to mitochondrial matrix via PiC may be a rate-limiting step for ATP production. However, precise detection of PiC and its significance in metabolism–secretion coupling in pancreatic β-cells has not been reported previously. In the present study, the role of PiC in metabolism–secretion coupling in pancreatic β-cells is evaluated using INS-1 cells manipulated to reduce PiC expression.

EXPERIMENTAL

Materials

ATP, ADP, poly-L-ornithine, DAPP (diadenosine pentaphosphate), Safranin O, FCCP (carbonyl cyanide *p*-trifluoromethoxyphenylhydrazone), ATP sulfurylase and Na_2MoO_4 were purchased from Sigma. Hepes, KCl, EGTA, sodium pyruvate, $MgSO_4$, NaH_2PO_4, $CaCl_2$, glucose, NaCl, $NaHCO_3$, $HClO_4$, Na_2CO_3, pyruvate kinase, BSA, KOH, potassium gluconate and KH_2PO_4 were purchased from Nacalai. 2-mercaptoethanol, penicillin, streptomycin and mouse monoclonal antibodies to the subunits of the mitochondrial respiratory chain complexes were purchased from Invitrogen. Luciferin-luciferase was purchased from Promega.

Cell culture

INS-1 (rat insulinoma) cells were cultured in RPMI 1640 medium containing 11.1 mM glucose (Invitrogen) supplemented with 10 % heat-inactivated fetal calf serum, 10 mM Hepes, 2 mM L-glutamine, 1 mM sodium pyruvate, 50 μM 2-mercaptoethanol, 100 IU/ml penicillin and 100 μg/ml streptomycin at 37 °C in a humidified atmosphere (5 % CO_2 and 95 % air). COS-7 (African green monkey kidney) cells were cultured in Dulbecco's modified Eagle's medium supplemented with 10 % heat-inactivated fetal calf serum, 100 IU/ml penicillin and 100 μg/ml streptomycin at 37 °C in a humidified atmosphere (5 % CO_2 and 95 % air).

siRNA transfection

Stealth™ siRNAs were synthesized by Invitrogen. The sequences of siRNAs specific for both rat PiC-A and PiC-B were: 5′-AAAUAUGCCCUUGUACUUCUGAGGG-3′ and 5′-CCCUCAGAAGUACAAGGGCAUAUUU-3′ designated as PiC siRNA1 and 5′-GAACACCUAUCUGUGGCGUACAUCA-3′ and 5′-UGAUGUACGCCACAGAUAGGUGUUC-3′ designated as PiC siRNA2. The sequences of control siRNAs were: 5′-ACCAACAACAGUUUGGGAAUAGGGA-3′ and 5′-UCCCUAUUCCCAAACUGUUGUUGGU-3′. Cultured INS-1 cells were trypsinized, suspended with RPMI 1640 medium without antibiotics, mixed with Opti-MEM (Invitrogen) containing siRNA and Lipofectamine™ 2000 (Invitrogen), plated on dishes or wells and then incubated at 37 °C in a CO_2 incubator. The final amounts of INS-1 cells, RPMI 1640, Opti-MEM, siRNA and Lipofectamine™ 2000 were 1×10^6 cells/ml, 75 % (v/v), 25 % (v/v), 80 nM and 0.3 % respectively. Medium was replaced with RPMI 1640 3–4 h after transfection. All experiments using siRNA-transfected INS-1 cells were performed 48 h after transfection unless otherwise noted.

Isolation of total RNA and quantitative RT (reverse transcription)–PCR

Total RNA was isolated from cardiac muscle, brain, skeletal muscle, kidney, liver and lung of Wistar rats using TRIzol® (Invitrogen) and from islets of Wistar rats and INS-1 cells using RNeasy mini kit (Qiagen). Animals were maintained and used in accordance with the Guidelines for Animal Experiments of Kyoto University. Islets were isolated by collagenase digestion [17]. cDNA was prepared by reverse transcriptase (Superscript II; Invitrogen) with an oligo(dT) primer. The rat sequences of forward and reverse primers to detect PiC-A, PiC-B, total PiC (PiC-A plus PiC-B) and β-actin (as an inner control) are shown in Table 1. AmpliTaq Gold (Applied Biosystems) was used as a DNA polymerase for RT–PCR. SYBR Green PCR Master Mix (Applied Biosystems) was prepared for the quantitative RT–PCR run. The thermal cycling conditions were denaturation at 95 °C for 10 min followed by 40 cycles at 95 °C for 30s and 60 °C for 30s.

Table 1 Primer sequences used in RT–PCR and quantitative RT–PCR

Name	Forward	Reverse
PiC-A	5′-AGCTGGTGCACGATGTGTCG-3′	5′-TTCCTCCGAGTCCACAGAGG-3′
PiC-B	5′-AGCTGGTGCACGATGTGTCG-3′	5′-CCACCAAAGCCACACAGTGC-3′
Total PiC (PiC-A+PiC-B)	5′-AGAGCAGCTGGTTGTGACAT-3′	5′-ACACCTCTAAAGCCAAGCCT-3′
β-actin	5′-CAATGAGCGGTTCCGATGCC-3′	5′-AATGCCTGGGTACATGGTGG-3′

Plasmid construction and transfection

The cDNA fragment of rat PiC-B was obtained from rat islets by RT–PCR and cloned into the pHMCA5 vector. pHMCA5-PiC-B was transfected into COS-7 and INS-1 cells using FuGENE™ 6 transfection reagent (Roche) and Lipofectamine™ 2000 respectively.

Immunoblot analysis

Rabbit antibody against the rat PiC peptide PPEM-PESLKKKLGLTE corresponding to C-terminal residues was originally raised. For immunoblotting, cells were washed with PBS containing protease inhibitor (Complete; Roche), suspended in 1 ml of PBS containing protease inhibitor and homogenized. Protein (50 μg per sample) was separated on a 15 % polyacrylamide gel and transferred to a nitrocellulose membrane. After blocking with TBS (Tris-buffered saline; 10 mM Tris/HCl and 100 mM NaCl, pH 7.5) containing 0.1 % Tween 20 and 5 % skimmed milk (blocking buffer) at room temperature (25 °C) for 2 h, blotted membranes were incubated overnight at 4 °C with anti-PiC antibody at 1:500 dilution, anti-DIC (dicarboxylate carrier) antibody (Novus Biologicals) at 1:100 dilution, mouse monoclonal anti-complex I (39 kDa subunit) antibody, anti-complex III (core II) antibody, anti-complex IV (subunit I) antibody or anti-complex V (subunit α) of mitochondrial respiratory chain antibody at 1:1000 dilution in blocking buffer, and subsequently with anti-rabbit (for PiC and DIC) or anti-mouse (for respiratory chain proteins) IgG horseradish peroxidase-conjugated secondary antibody (GE Healthcare) diluted 1:5000 at room temperature for 2 h prior to detection using ECL (GE Healthcare). In the same membrane, the process was repeated for β-actin at 1:1000 dilution of the antibody. Band intensities were quantified with Multi Gauge software (Fujifilm).

Insulin secretion

For insulin secretion assays, INS-1 cells cultured on 24-well plates coated with 0.001 % poly-L-ornithine were washed with KRBH (Krebs-Ringer bicarbonate Hepes buffer) composed of

140 mM NaCl, 3.6 mM KCl, 0.5 mM $MgSO_4$, 0.5 mM NaH_2PO_4, 1.5 mM $CaCl_2$, 2 mM $NaHCO_3$, 0.1 % BSA and 10 mM Hepes (pH 7.4) with 2 mM glucose, preincubated at 37 °C for 30 min in KRBH with 2 mM glucose, and then incubated at 37 °C for 30 min in KRBH with 2 mM glucose, 10 mM glucose or 2 mM glucose plus 30 mM KCl. Insulin concentrations were determined by RIA using rat insulin as a standard as previously described [17].

Adenine nucleotides

ATP and ADP contents were determined as previously described [18,19] with some modifications. Briefly, INS-1 cells were cultured, washed and preincubated as described above and incubated with KRBH with 2 mM glucose, 10 mM glucose or 2 mM glucose plus 30 mM KCl at 37 °C for 30 min. Incubation was stopped by the addition of $HClO_4$. The contents of wells were sonicated [three pulses of 3 s duration using a Handy Sonic UR-20P instrument (TOMY SEIKO) on ice] and transferred into glass tubes. The tubes were then centrifuged, and a fraction of the supernatant was neutralized with Hepes and Na_2CO_3. The ATP concentration was measured by luciferin-luciferase assay. After ATP in the neutralized extract was irreversibly converted to AMP with ATP sulfurylase in the presence of Na_2MoO_4, ADP in the reactant was converted to ATP with pyruvate kinase and was determined by luciferin-luciferase assay as the difference between the measurements with and without pyruvate kinase.

Intracellular calcium concentration ($[Ca^{2+}]_i$) and mitochondrial membrane potential ($\Delta\psi_m$) in living cells

INS-1 cells were seeded on to glass coverslips coated with 0.001 % poly-L-ornithine and cultured 48 h before measurements were made. For measurements of $[Ca^{2+}]_i$, cultured INS-1 cells were loaded with 5 μM Fura-PE3/AM (Calbiochem) at 37 °C for 90 min, placed in a heat-controlled chamber on the stage of an inverted microscope kept at 36 ± 1 °C, superfused with KRBH containing 2 mM glucose, and subsequently exposed to the buffer containing 10 mM glucose or 30 mM KCl. The cells were excited successively at 340 and 380 nm, and the fluorescence emitted at 510 nm was captured by CCD camera (Micro Max 5 MHz System, Roper Industries, Trenton, NJ). The images were analysed with the Meta Fluor image analyzing system (Universal Imaging). The 340 nm (F340) and 380 nm (F380) fluorescence signals were detected every 15 s, and ratios (F340/F380) were calculated. For $\Delta\psi_m$ measurements, the same protocol as above was used except that cultured cells were loaded with 10 μg/ml rhodamine 123 (Invitrogen) at 37 °C for 30 min and fluorescence excited at 490 nm and emitted at 530 nm every 20 s was monitored.

ATP production and $\Delta\psi_m$ in mitochondrial fraction

Measurement of ATP production from the mitochondrial fraction was performed as previously described [18] with minor modifications. Firstly, INS-1 cells were homogenized in solution A consisting of 50 mM Hepes, 100 mM KCl, 1.8 mM ATP, 1 mM EGTA, 2 mM $MgCl_2$ and 0.5 mg/ml BSA (electrophoretically homogeneous) with the pH adjusted to 7.00 at 37 °C with KOH. After precipitation of cell debris and nuclei by 800 g centrifugation for 3 min, the supernatant was centrifuged more rapidly (10000 g for 3 min) to obtain a pellet containing the mitochondrial fraction. The precipitation, diluted by 200 μl of solution A, was centrifuged again and rinsed three times in solution B, consisting of 20 mM Hepes, 1 mM EGTA, 12 mM NaCl, 0.3 mM $MgCl_2$, 130 mM potassium gluconate and 0.5 mg/ml BSA (electrophoretically homogeneous) with the pH adjusted to 7.10 with KOH. The mitochondrial fraction in 500 μl of solution B was kept on ice until use. To measure ATP production by oxidative phosphorylation, the reaction was started by adding mitochondrial suspension to prewarmed solution B (37 °C) containing mitochondrial substrates with or without respiratory chain inhibitors, 50 μM ADP, 1 μM DAPP and various levels of P_i. DAPP, a specific inhibitor of adenylate kinase, was used to measure ATP production by oxidative phosphorylation exclusively. After the reaction was stopped, the ATP concentration in the solutions was measured by adding luciferin-luciferase solution with a bioluminometer. ATP production was corrected by mitochondrial protein content. Measurement of $\Delta\psi_m$ was performed as previously described [20] with some modifications. Fluorescence was successively monitored using a spectrofluorophotometer (RF 5000; Shimadzu) with an excitation wavelength of 495 nm and emission at 586 nm, and with stirring solution B supplemented with 3 mM KH_2PO_4, 50 μM ADP and 2.5 μM Safranin O applied in a glass cuvette at 37 °C. Mitochondria, succinate and FCCP were added to the solution in this order and final concentrations were 50 μg/ml, 1 mM and 200 nM respectively.

Statistical analysis

The data are expressed as means $\pm$ S.E.M. Statistical significance was calculated by unpaired Student's t test. $P < 0.05$ was considered significant.

RESULTS

Expression of PiC mRNA in pancreatic β-cells

Tissue distribution of PiC was evaluated by RT–PCR (Figure 1A). PiC-B was expressed ubiquitously whereas PiC-A was expressed clearly in cardiac muscle and skeletal muscle as previously reported [13,14] and obscurely in rat islets and INS-1 cells. These results indicate that PiC-B was dominantly expressed in pancreatic β-cells.

Evaluation of anti-PiC antibody

The cell lysates of COS-7 cells transfected with pHMCA5-PiC or pHMCA5-null, INS-1 cells transfected with pHMCA5-null, intact INS-1 cells and rat islets were electrophoresed and immunoblotted using the anti-PiC antibody. As shown in Figure 1(B), the band at ~30 kDa, which was not detected in COS-7 cells transfected with pHMCA5-null, was detected in COS-7 cells transfected with pHMCA5-PiC, INS-1 cells transfected with pHMCA5-null, intact INS-1 cells and rat islets. This observation is consistent with a previous report that rat PiC was detected at ~30 kDa by an antibody originally raised using the C-terminal amino acids as the antigen peptide [21].

Silencing effects of PiC siRNAs on INS-1 cells

Quantitative RT–PCR assays using primers for total PiC (PiC-A plus PiC-B, Table 1) and immunoblotting using anti-PiC antibody revealed ~70 % reduction of PiC mRNA expression and ~40 % reduction of the protein expression in INS-1 cells 48 h after both PiC siRNA1 and 2 transfection respectively (Figures 1C and 1D). Time-dependent reduction of PiC protein expression (~25 %, ~40 % and ~50 % reduction at 24 h, 48 h and 72 h after siRNA1 and 2 transfection) implies long half-life of PiC, which causes low efficacy of suppression (Figure 1D). Transfection of control siRNA did not affect the expression of PiC in INS-1 cells at both mRNA and protein levels. Protein expressions of DIC,

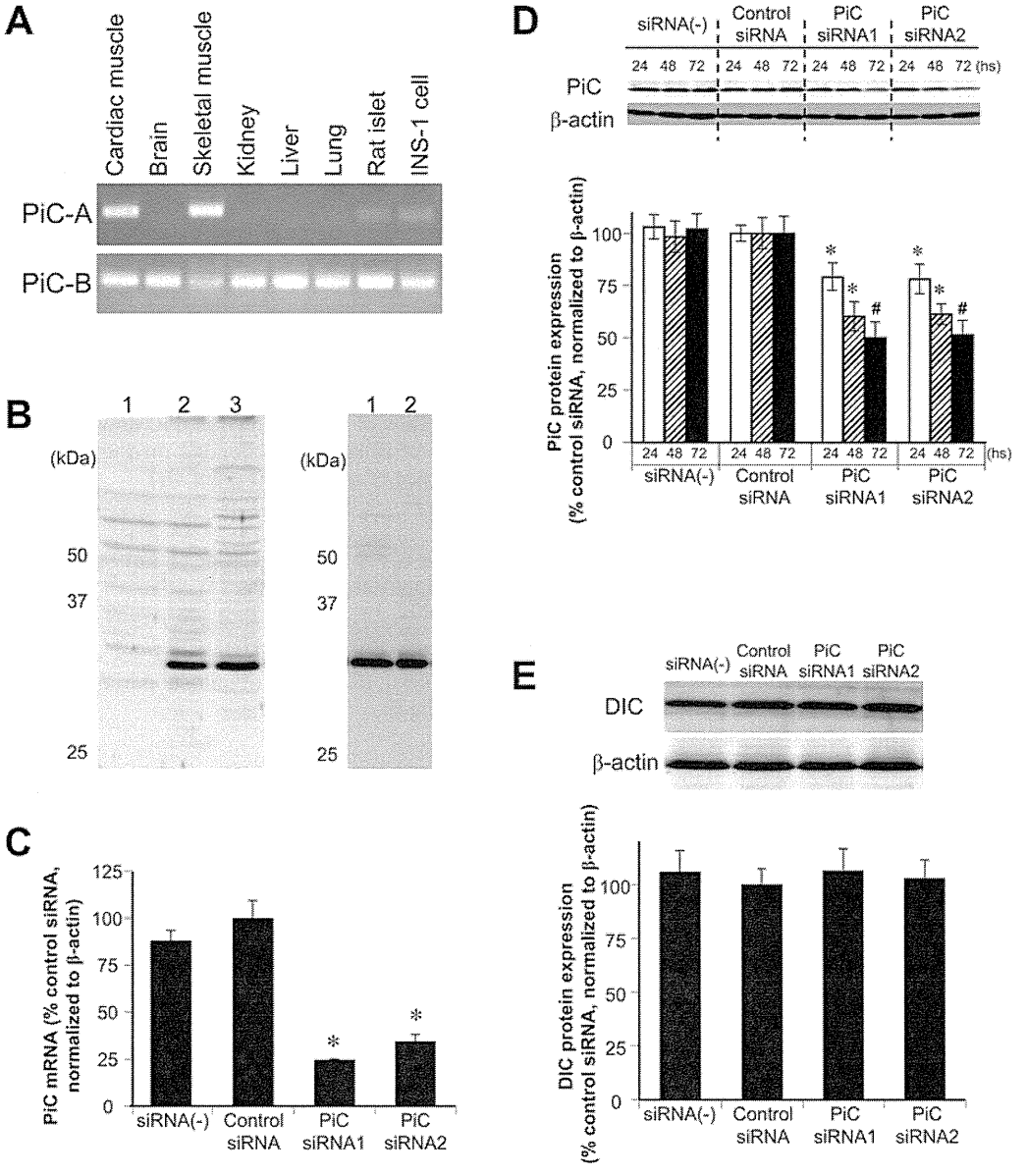

Figure 1 Detection of rat PiC and silencing effects of PiC siRNAs on INS-1 cells

(**A**) RT–PCR detection of PiC mRNA expression in various rat tissues and INS-1 cells. PiC mRNA expressions in cardiac muscle, brain, skeletal muscle, kidney, liver, lung and islets of Wistar rat and INS-1 cells were evaluated with RT–PCR using primers of specific sequences for PiC-A and PiC-B. Product sizes are 141 bp for PiC-A and 136 bp for PiC-B. (**B**) Evaluation of anti-PiC antibody by immunoblot analysis. Left panel: whole cell lysates from COS-7 cells transfected with pHMCA5-null (lane 1), COS-7 cells transfected with pHMCA5-PiC (lane 2) and INS-1 cells transfected with pHMCA5-null (lane 3) were electrophoresed and immunoblotted with anti-PiC antibody. Right panel: whole cell lysates from INS-1 cells (lane 1) and rat islets (lane 2) were electrophoresed and immunoblotted with anti-PiC antibody. Molecular mass in kDa is given on the left-hand side of each panel. (**C**) Effects of transfection of PiC siRNAs on the expression of PiC mRNA was evaluated with quantitative RT–PCR using a pair of primers recognizing both PiC-A and PiC-B (total PiC). Data were normalized using β-actin mRNA. $n = 3$ in each group. $^*P < 0.01$ compared with control siRNA. (**D**) Immunoblot analysis of PiC expression revealed that PiC siRNAs reduced PiC expression in INS-1 cells. Time (h) after siRNA transfection is indicated. Data were normalized by the expression of β-actin. $n = 4$ in each bar. $^*P < 0.05$ and $\#P < 0.01$ compared with control siRNA. (**E**) Effects of PiC silencing on expression of DIC. Whole INS-1 cell lysate was electrophoresed and immunoblotted using antibodies against DIC. Quantification data were obtained from four independent experiments and normalized with β-actin levels.

another P_i carrier, were not affected by siRNA1 and 2 transfection (Figure 1E).

Effects of PiC down-regulation on glucose- and depolarization-stimulated insulin secretion

Down-regulation of PiC decreased GSIS (10 mM glucose) in INS-1 cells, as shown in Figure 2. A reduction in GSIS of 61 % by PiC siRNA1 and 47 % by PiC siRNA2 was observed. K^+ (30 mM)-stimulated insulin secretion was also reduced: the reduction was 27 % by PiC siRNA1 and 23 % by PiC siRNA2, which were milder than those of GSIS (Figure 2). Insulin secretion in the basal glucose state (2 mM) was not affected by PiC siRNA1, but was slightly increased by PiC siRNA2. Transfection of control siRNA did not affect GSIS in INS-1 cells.

Effects of PiC down-regulation on adenine nucleotides

Down-regulation of PiC increased ADP and decreased the ATP:ADP ratio, whereas it did not significantly affect ATP in

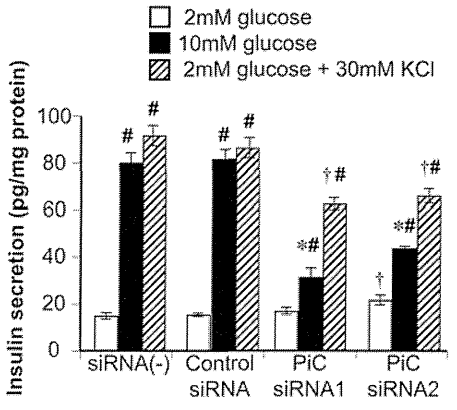

Figure 2 Effects of PiC down-regulation on glucose- or KCl-stimulated insulin secretion

INS-1 cells were incubated for 30 min with 2 mM glucose, 10 mM glucose or 2 mM glucose and 30 mM K^+, and insulin secretion was measured. Data were obtained from six independent experiments normalized by protein concentration. Error bars are means ± S.E.M. *$P < 0.01$ and †$P < 0.05$ compared with control siRNA at the corresponding condition. #$P < 0.01$ compared with corresponding 2 mM glucose.

the presence of 10 mM glucose in INS-1 cells (Table 2A). ATP, ADP and the ATP:ADP ratio at 2 mM glucose was not altered by silencing PiC (Tables 2A and 2B). Depolarization evoked by 30 mM K^+ in the presence of 2 mM glucose decreased the ATP:ADP ratio in both control and PiC down-regulated cells, whereas suppression of the ATP:ADP ratio was lower in PiC down-regulated cells compared with control cells (Table 2B).

Effects of PiC down-regulation on $[Ca^{2+}]_i$ and $\Delta\psi_m$ in living cells

Fluorescence signals of Fura-PE3 revealed that elevation of $[Ca^{2+}]_i$ in response to a stimulating level of 10 mM glucose was decreased and delayed by PiC down-regulation compared with that in control (Figure 3A). Average values calculated using the data from Figure 3(A) also indicate that PiC siRNA reduced the mean $[Ca^{2+}]_i$ at 10 mM glucose (PiC siRNA1, 0.864 ± 0.004 compared with control siRNA, 0.896 ± 0.003; $P < 0.01$) whereas there was no significant change at basal (2 mM) glucose (PiC siRNA1, 0.846 ± 0.004; control siRNA, 0.857 ± 0.003), as shown in Figure 3(B). Elevation of $[Ca^{2+}]_i$ in response to 30 mM K^+ was slightly decreased by PiC siRNA1 (average value of Fura-PE3 fluorescence ratio was 0.968 ± 0.005, compared with a control siRNA ratio of 0.991 ± 0.005, $P < 0.01$) without affecting basal value (control siRNA, 0.857 ± 0.006; siRNA1, 0.854 ± 0.004) as shown in Figures 3(C) and 3(D). Fluorescence measurement using rhodamine 123 demonstrated that the mitochondrial membrane in INS-1 cells was hyperpolarized by raising glucose from 2 to 10 mM and prominently depolarized by FCCP, and that PiC down-regulation did not affect glucose-induced hyperpolarization and total depolarization after FCCP exposure of $\Delta\psi_m$ throughout the measurement (Figure 3E).

Effects of PiC down-regulation on ATP production and $\Delta\psi_m$ in mitochondrial fraction

ATP production by mitochondria from INS-1 cells transfected with control or PiC siRNAs in the presence of 1 mM succinate and various concentrations of P_i ($[P_i]$) is shown in Figure 4(A). PiC down-regulation decreased mitochondrial ATP production by 50–60 % at $[P_i]$ ranging from 0.001 to 10 mM. ATP production in all groups reached maximum rates above ~3 mM of $[P_i]$, which indicates that the PiC amount regulates the maximal rate of mitochondrial ATP production. On the other hand, K_m values of $[P_i]$ for ATP production were similar (~0.05 mM). Mitochondrial ATP production in the presence of various mitochondrial substrates and inhibitors of the respiratory chain is shown in Table 3. ATP production in the presence of succinate was completely inhibited by antimycin A, a complex III inhibitor, in both control and PiC down-regulated INS-1 cells. PiC siRNAs decreased ATP production in the presence of pyruvate and malate by 42–58 %, succinate plus rotenone by 46–62 % and TMPD (*N*,*N*,*N*′,*N*′-tetramethyl-*p*-phenylenediamine) plus ascorbate by 61–62 %, showing that ATP production by electrons rendered at complex I, complex II and complex IV is suppressed to a similar degree. In spite of significant down-regulation of ATP production, PiC down-regulation did not affect $\Delta\psi_m$ of isolated mitochondria measured with Safranin O in the presence of succinate (Figure 4B).

Effects of PiC down-regulation on expression of mitochondrial respiratory chain proteins

Immunoblotting using lysates of whole INS-1 cells revealed that transfection of PiC siRNAs did not change the expression of complex I, III, IV or V of mitochondrial respiratory chain proteins (Figure 5).

DISCUSSION

In the present study, the mitochondrial phosphate carrier (PiC) was revealed to play an important role in metabolism–secretion coupling of pancreatic β-cells by using INS-1 cells and PiC siRNA. PiC down-regulation brings about reduction in mitochondrial ATP production by mitochondrial fuels, resulting in reduced glucose-induced $[Ca^{2+}]_i$ elevation and impaired GSIS.

In pancreatic β-cells, ATP increase is slight and ADP decrease is prominent via an increase in glucose levels beyond the triggering level of insulin secretion. In addition, the ATP/ADP ratio is well-correlated with GSIS rather than the absolute value of ATP [22,23]. PiC down-regulation decreased the ATP/ADP ratio in the presence of high glucose, which causes insufficient closure of K_{ATP} channels, a decrease in $[Ca^{2+}]_i$ elevation by glucose (Figures 3A and 3B), and suppression of GSIS (Figure 2).

Insulin secretion at 10 mM glucose was similar to that at 30 mM K^+ and 2 mM glucose in the control samples. In contrast, in PiC down-regulated INS-1 cells, GSIS is lower than depolarization-induced insulin secretion, which suggests specific effects of PiC on metabolism–secretion coupling (Figure 2). However, ~25 % suppression of depolarization-induced insulin secretion, which is modest compared with GSIS, was observed in PiC down-regulated INS-1 cells. Measurements revealed that $[Ca^{2+}]_i$ in the presence of 2 mM glucose and 30 mM K^+ was reduced by PiC down-regulation (Figures 3C and 3D), which plays a role in reduced depolarization-induced insulin secretion by PiC down-regulation. Depolarization reduced the ATP/ADP ratio in the presence of a basal level of glucose in control samples, which accords with a previous study where an increase in $[Ca^{2+}]_i$ causes a larger consumption than production of ATP [24] (Table 2B). The ATP/ADP ratio was also reduced by depolarization at 2 mM glucose in PiC down-regulated INS-1 cells, although the suppression was lower than that in control samples, which may reflect a smaller elevation of $[Ca^{2+}]_i$ than in the control. In addition, in contrast with a significant suppression of the ATP/ADP ratio at high glucose concentrations by PiC down-regulation, in the presence of a basal

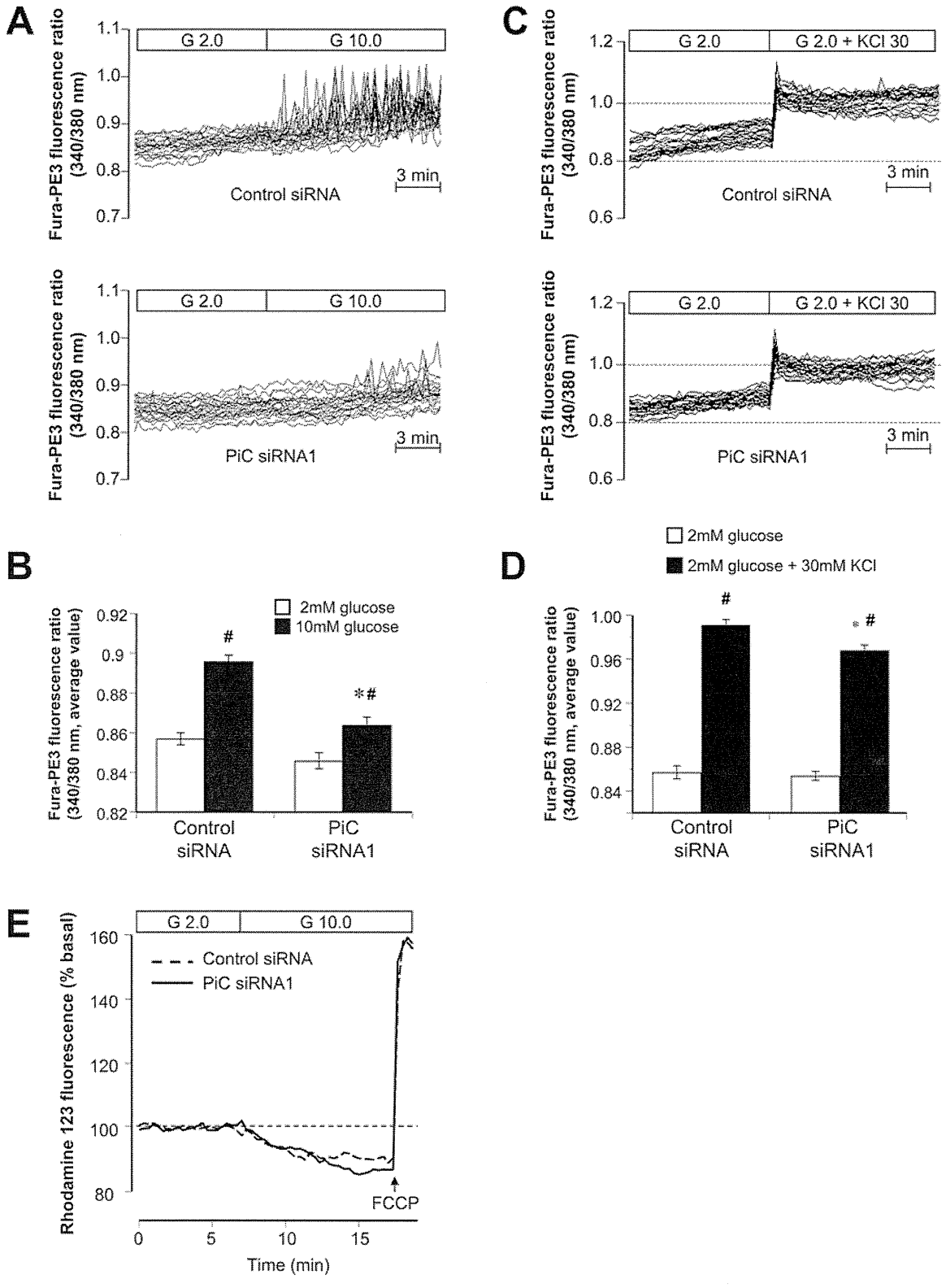

Figure 3 Effects of PiC down-regulation on $[Ca^{2+}]_i$ and $\Delta\psi_m$ in living cells

(**A**) $[Ca^{2+}]_i$ elevation and oscillation induced by raising glucose (G) from 2 to 10 mM were monitored in INS-1 cells transfected with PiC siRNA. Traces of Fura-PE3 fluorescence ratio (340/380 nm) were obtained from 20 cells of each group. (**B**) Average values calculated from the data from (**A**). $*P < 0.01$ compared with control siRNA at 10 mM glucose. $\#P < 0.01$ compared with corresponding 2 mM glucose. (**C**) $[Ca^{2+}]_i$ elevation induced by 30 mM KCl was monitored in INS-1 cells transfected with PiC siRNA. Traces of Fura-PE3 fluorescence ratio (340/380 nm) were obtained from 20 cells of each group. (**D**) Average values calculated from the data from (**C**). $*P < 0.05$ compared with control siRNA at 30 mM KCl. $\#P < 0.01$ compared with corresponding 2 mM glucose. (**E**) $\Delta\psi_m$ monitored by rhodamine 123 fluorescence in INS-1 cells. Data were corrected with the average values of fluorescence under basal glucose (2 mM) conditions. $n = 10$. Error bars are means$\pm$S.E.M.

Table 2 Effects of PiC down-regulation on adenine nucleotides

(A)

	Control siRNA		PiC siRNA1		PiC siRNA2	
Glucose (mM)	2	10	2	10	2	10
ATP (nmol/mg protein)	65.2 ± 3.8	77.4 ± 3.8*	64.4 ± 1.0	71.8 ± 3.3*	66.2 ± 1.7	80.0 ± 5.5*
ADP (nmol/mg protein)	10.2 ± 0.6	3.9 ± 0.4†	10.6 ± 0.6	6.4 ± 0.9*‡	9.7 ± 0.6	6.1 ± 1.2*‡
ATP/ADP	6.5 ± 0.6	20.5 ± 2.0†	6.1 ± 0.4	12.0 ± 1.7*‡	6.9 ± 0.5	13.9 ± 1.4*‡

(B)

	Control siRNA			PiC siRNA1	
Glucose (mM)	2	2	2	2	2
K^+ (mM)	3.6	30	3.6	3.6	30
Antimycin A (μM)	0	0	1	0	0
ATP (nmol/mg protein)	65.5 ± 3.4	48.6 ± 1.9*	2.5 ± 0.1†	64.4 ± 4.7	61.2 ± 1.8‡
ADP (nmol/mg protein)	10.1 ± 0.1	11.2 ± 0.2*	10.5 ± 0.1*	9.9 ± 0.2	10.5 ± 0.3*‡
ATP/ADP	6.5 ± 0.3	4.4 ± 0.2†	0.2 ± 0.0†	6.5 ± 0.5	5.8 ± 0.2*§

*$P < 0.05$ and †$P < 0.01$ compared with basal condition (2 mM glucose). ‡$P < 0.05$ and §$P < 0.01$ compared with control siRNA. Data were obtained from four independent experiments.

Table 3 Silencing effects of PiC siRNAs on ATP production from mitochondrial fraction of INS-1 cells

	Mitochondrial ATP production (μmol/10 min per mg of protein)		
Experimental conditions	Control siRNA	PiC siRNA1	PiC siRNA2
1 mM succinate	1.28 ± 0.02	0.61 ± 0.02*	0.46 ± 0.01*
1 mM succinate + 1 μM rotenone	1.03 ± 0.09	0.56 ± 0.03*	0.39 ± 0.01*
1 mM succinate + 1 μM antimycin A	0.03 ± 0.01	0.00 ± 0.01	0.00 ± 0.01
1 mM pyruvate + 1 mM malate	0.41 ± 0.03	0.24 ± 0.01*	0.17 ± 0.00*
0.5 mM TMPD + 2 mM ascorbate	3.43 ± 0.09	1.33 ± 0.03*	1.27 ± 0.01*

*$P < 0.01$ compared with control siRNA. Data were obtained from three independent experiments.

level of glucose, PiC down-regulation did not affect the ATP/ADP ratio in INS-1 cells. An incomplete compensatory effect derived from PiC down-regulation, which is valid in a basal supply of substrate to mitochondria but deteriorates in an accelerated supply at high glucose, might save ATP consumption and maintain the basal ratio of ATP/ADP.

PiC, which is required for mitochondrial ATP production, has two isoforms. PiC-A is expressed in skeletal and cardiac muscle whereas PiC-B is expressed ubiquitously. AAC (ATP/ADP carrier), which is also required for mitochondrial ATP production, has isoforms including AAC1 (SLC25A4), AAC2 (SLC25A5) and AAC3 (SLC25A6). Interestingly, these isoforms, except AAC2, expression of which is absent or scarce in most tissues, distribute similarly to the PiC isoforms: AAC1 is expressed in skeletal and cardiac muscle, and AAC3 is expressed ubiquitously. These distributions imply that ubiquitously-expressed PiC-B and AAC3 may meet stable energy requirement, and PiC-A and AAC1, which are expressed exclusively in muscle, meet higher and prompt energy demands for muscle contraction. In the present study, we demonstrate that PiC-B is the dominant isoform of PiC whereas PiC-A is scarcely expressed in INS-1 cells and rat islets (Figure 1A), which may reflect less prompt energy demand in β-cells compared with that in muscles.

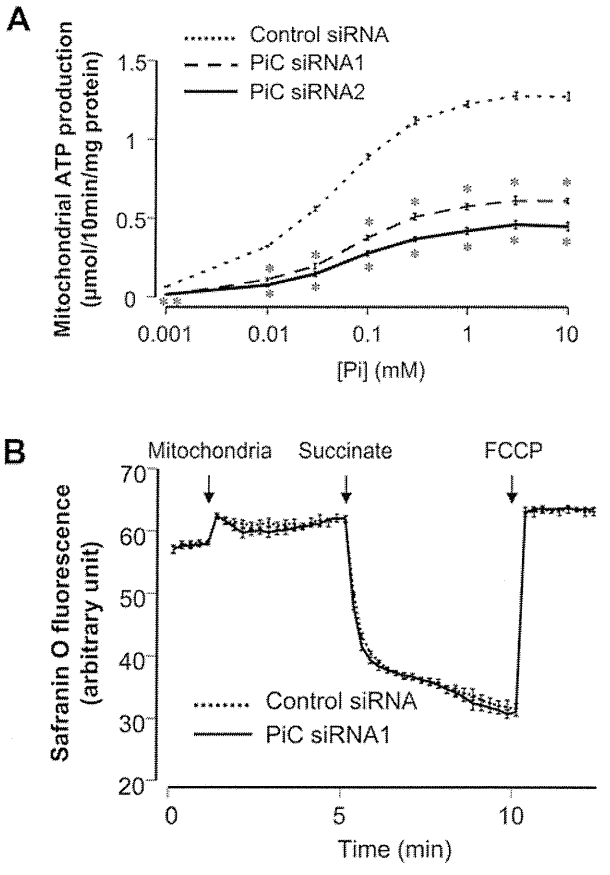

Figure 4 Effects of PiC down-regulation on ATP production and $\Delta\psi_m$ in mitochondrial fraction isolated from INS-1 cells

(**A**) Effects of PiC down-regulation on mitochondrial ATP production at various phosphate concentrations. ATP production was evaluated in mitochondria isolated from INS-1 cells in the presence of 50 μM ADP, 1 μM DAPP and 1 mM succinate with various concentrations of P_i indicated in the Figure. $n = 3$ in each plot. *$P < 0.01$ compared with control siRNA. (**B**) $\Delta\psi_m$ monitored by Safranin O fluorescence. Mitochondria (50 μg/ml), succinate (1 mM) and FCCP (200 nM) were added to the solution containing Safranin O at the points indicated with arrows. $n = 4$ in each group.

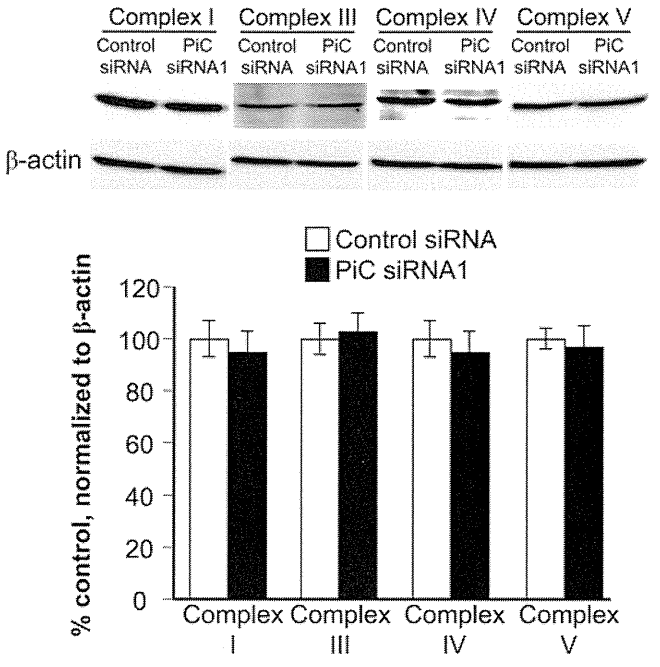

Figure 5 Effects of PiC silencing on expression of mitochondrial respiratory chain proteins

Lysates of whole INS-1 cells were electrophoresed and immunoblotted using antibodies against complex I, III, IV and V. Quantification data were obtained from four independent experiments and normalized with β-actin levels. Error bars are means±S.E.M.

Mitochondrial ATP is produced by complex V (ATP synthase), which is driven by protonmotive force generated by proton extrusion during transport of high-energy electrons in the respiratory chain. In the present study, mitochondrial ATP production in the presence of mitochondrial fuel increased according to the raised extramitochondrial phosphate concentration ($[P_i]_e$), and reached maximum rate above ~3 mM of $[P_i]_e$, which was decreased by 50–60 % without affecting the K_m value of $[P_i]_e$ for ATP production by ~40 % reduction in PiC protein. The physiological intracellular $[P_i]$ in heart determined by methods including ^{31}P NMR is ~1 mM at rest and increases to ~10 mM depending on the metabolic state [25–27]. Levels of P_i in islets are ~20 mmol/kg of dry weight tissue [28], which corresponds to ~10 mM by conversion [29]. Taken together, the rate of mitochondrial ATP production might be barely affected by a physiological change of $[P_i]_e$ but be evidently affected by alteration of the amount of PiC protein. In addition, reduction in ATP production by down-regulation of PiC also suggests that compensatory supply of P_i to mitochondria by other mitochondrial phosphate carriers including DIC (SLC25A10) [30,31] does not occur, which is supported by no apparent effect of PiC down-regulation on DIC expression (Figure 1E). These results accord with the first description that PiC dysfunction impairs the synthesis of ATP [15].

Intramitochondrial P_i is thought to affect oxidative phosphorylation at multiple sites [16]. To find specific defective sites in the respiratory chain in PiC down-regulated INS-1 cells, mitochondrial ATP production was examined in the presence of various substrates and inhibitors. Pyruvate and malate, which are metabolized in mitochondria to generate NADH, render electrons at complex I. In the presence of rotenone, a complex I inhibitor, succinate renders electrons directly to complex II via $FADH_2$. TMPD is an artificial electron donor that can transfer electrons to cytochrome *c*. TMPD reduced by ascorbate renders electrons to cytochrome *c*, which transfers electrons to complex IV. Reduction of ATP production by down-regulation of PiC in the presence of pyruvate plus malate, succinate plus rotenone and TMPD plus ascorbate were all suppressed similarly by 50–60 % (Table 3). These results indicate that reduction in ATP production by down-regulation of PiC may well be derived from a defective site downstream of complex IV and that a defective site upstream of complex IV, if present, does not play a prominent role. Moreover, immunoblotting revealed that expressions of respiratory chain proteins including complex I, III, IV and V were not affected by PiC silencing. Considered together, silencing of PiC seems to suppress mitochondrial ATP production not by affecting mitochondrial biogenesis, but by restricting P_i supply to complex V.

Inhibition of complex V by oligomycin reduces ATP production with hyperpolarization of $\Delta\psi_m$ [32,33], which may be derived from the fact that complex V is a protonophore and its inhibition affects electrogenic H^+ influx to mitochondria specifically and directly affects $\Delta\psi_m$. In contrast, PiC is electroneutral due to symport of H^+ and negatively charged P_i or antiport of OH^- and negatively charged P_i and does not directly affect $\Delta\psi_m$. ATP generation in complex V is driven by protonmotive force (Δp), which has two components: electrical membrane potential ($\Delta\psi_m$) and the difference between the cytosolic and matrix pH (ΔpH) [34,35]. P_i plays regulatory roles in oxidative phosphorylation by affecting Δp. An increase in $[P_i]_e$ reduces ΔpH [34,36–38] due to an increase in co-transport of P_i and protons from cytosol into mitochondrial matrix through PiC. On the other hand, $\Delta\psi_m$ is increased by an increase in $[P_i]_e$ of less than ~2 mM, but reaches a plateau at $[P_i]_e$ above ~2 mM [16,34,38]. Increases in $\Delta\psi_m$ owing to increases in $[P_i]_e$ is not fully elucidated, but some explanations are proposed. An electroneutral influx of protons (H^+) accompanying negatively charged substrates such as P_i does not directly affect $\Delta\psi_m$ but produces a reduction in ΔpH that promotes proton extrusion by the respiratory chain to maintain Δp and eventually increases $\Delta\psi_m$ [35]. Bose et al. [16] provided another explanation: an increase in the influx of P_i activates intramitochondrial NADH production and NADH supply to complex I and also promotes the ability to generate Δp by improving the coupling of electron transport between cytochrome *b* and cytochrome *c*, which eventually increases $\Delta\psi_m$. Interestingly, in the present study, ~40 % reduction in the protein level of PiC did not affect glucose-induced hyperpolarization of the mitochondrial inner membrane in spite of a reduction in ATP production. It is possible that the reduction in P_i influx by down-regulation of PiC in the present study is within a range of P_i influx which does not affect $\Delta\psi_m$ as with higher $[P_i]_e$. In addition, our results were derived from sustained down-regulation of P_i influx to mitochondria, as experiments were performed 48 h after transfection of PiC siRNA in contrast with the acute alteration of P_i influx by manipulation of $[P_i]_e$ in previous studies, which may permit adaptation of $\Delta\psi_m$ to maintain Δp.

It has been generally reported that the contribution of $\Delta\psi_m$ to Δp is 80–85 % [34,35,37–45] or more [16] and that of ΔpH is relatively small, which indicates that the alteration in Δp by down-regulation of PiC in the present study is small considering the non-detectable affect on $\Delta\psi_m$. Therefore the supply of P_i to complex V may well be a critical rate-limiting step for ATP production independent of Δp. The results in the present study demonstrate the critical role of P_i influx to mitochondria in ATP production and metabolism–secretion coupling in pancreatic β-cells.

AUTHOR CONTRIBUTION

Yuichi Nishi researched data, contributed to the discussion, wrote the manuscript and revised/edited the manuscript. Shimpei Fujimoto contributed to the discussion, wrote the manuscript and revised/edited the manuscript. Mayumi Sasaki, Eri Mukai, Hiroki Sato, Yuichi Sato, Yumiko Tahara and Yasuhiko Nakamura researched data. Nobuya Inagaki contributed to the discussion and revised/edited the manuscript.

ACKNOWLEDGEMENTS

We greatly appreciate the gifts of INS-1 cells from Dr Nobuo Sekine (Tokyo Kosei Nenkin Hospital, Tokyo, Japan) and pHMCA5 vector from Dr Hiroyuki Mizuguchi (National Institute of Biomedical Innovation, Ibaraki, Japan). We thank Mr Shinsaku Akagi, Mr Takuro Yamaguchi, Ms Chiyo Kotake and Ms Sara Yasui for technical assistance and Mr Eiji Yoshihara for helpful advice on siRNA transfection.

FUNDING

This study was supported by a Research Grant on Nanotechnical Medicine from the Ministry of Health, Labour, and Welfare of Japan, Scientific Research Grants, a grant from Innovation Cluster Kansai project of the Ministry of Education, Culture, Sports, Science and Technology of Japan, and a grant from CREST (Core Research for Evolutional Science and Technology) of Japan Science and Technology Cooperation.

REFERENCES

1 Maechler, P. and Wollheim, C. B. (2001) Mitochondrial function in normal and diabetic β-cells. Nature **414**, 807–812
2 Kennedy, E. D., Maechler, P. and Wollheim, C. B. (1998) Effects of depletion of mitochondrial DNA in metabolism secretion coupling in INS-1 cells. Diabetes **47**, 374–380
3 Tsuruzoe, K., Araki, E., Furukawa, N., Shirotani, T., Matsumoto, K., Kaneko, K., Motoshima, H., Yoshizato, K., Shirakami, A., Kishikawa, H. et al. (1998) Creation and characterization of a mitochondrial DNA-depleted pancreatic β-cell line: impaired insulin secretion induced by glucose, leucine, and sulfonylureas. Diabetes **47**, 621–631
4 Palmieri, F. (2004) The mitochondrial transporter family (SLC25): physiological and pathological implications. Pflugers Arch. **447**, 689–709
5 Rubi, B., del Arco, A., Bartley, C., Satrustegui, J. and Maechler, P. (2004) The malate-aspartate NADH shuttle member Aralar1 determines glucose metabolic fate, mitochondrial activity, and insulin secretion in beta cells. J. Biol. Chem. **279**, 55659–55666
6 Casimir, M., Rubi, B., Frigerio, F., Chaffard, G. and Maechler, P. (2009) Silencing of the mitochondrial NADH shuttle component aspartate-glutamate carrier AGC1/Aralar1 in INS-1E cells and rat islets. Biochem. J. **424**, 459–466
7 Chan, C. B., MacDonald, P. E., Saleh, M. C., Johns, D. C., Marban, E. and Wheeler, M. B. (1999) Overexpression of uncoupling protein 2 inhibits glucose-stimulated insulin secretion from rat islets. Diabetes **48**, 1482–1486
8 Zhang, C. Y., Baffy, G., Perret, P., Krauss, S., Peroni, O., Grujic, D., Hagen, T., Vidal-Puig, A. J., Boss, O., Kim, Y. B. et al. (2001) Uncoupling protein-2 negatively regulates insulin secretion and is a major link between obesity, β cell dysfunction, and type 2 diabetes. Cell **105**, 745–755
9 Odegaard, M. L., Joseph, J. W., Jensen, M. V., Lu, D., Ilkayeva, O., Ronnebaum, S. M., Becker, T. C. and Newgard, C. B. (2010) The mitochondrial 2-oxoglutarate carrier is part of a metabolic pathway that mediates glucose- and glutamine-stimulated insulin secretion. J. Biol. Chem. **285**, 16530–16537
10 Joseph, J. W., Jensen, M. V., Ilkayeva, O., Palmieri, F., Alarcon, C., Rhodes, C. J. and Newgard, C. B. (2006) The mitochondrial citrate/isocitrate carrier plays a regulatory role in glucose-stimulated insulin secretion. J. Biol. Chem. **281**, 35624–35632
11 Casimir, M., Lasorsa, F. M., Rubi, B., Caille, D., Palmieri, F., Meda, P. and Maechler, P. (2009) Mitochondrial glutamate carrier GC1 as a newly identified player in the control of glucose-stimulated insulin secretion. J. Biol. Chem. **284**, 25004–25014
12 Dolce, V., Iacobazzi, V., Palmieri, F. and Walker, J. E. (1994) The sequences of human and bovine genes of the phosphate carrier from mitochondria contain evidence of alternatively spliced forms. J. Biol. Chem. **269**, 10451–10460
13 Fiermonte, G., Dolce, V. and Palmieri, F. (1998) Expression in *Escherichia coli*, functional characterization, and tissue distribution of isoforms A and B of the phosphate carrier from bovine mitochondria. J. Biol. Chem. **273**, 22782–22787
14 Dolce, V., Fiermonte, G. and Palmieri, F. (1996) Tissue-specific expression of the two isoforms of the mitochondrial phosphate carrier in bovine tissues. FEBS Lett. **399**, 95–98
15 Mayr, J. A., Merkel, O., Kohlwein, S. D., Gebhardt, B. R., Böhles, H., Fötschl, U., Koch, J., Jaksch, M., Lochmüller, H. and Horváth, R. et al. (2007) Mitochondrial phosphate-carrier deficiency: a novel disorder of oxidative phosphorylation. Am. J. Hum. Genet. **80**, 478–484
16 Bose, S., French, S., Evans, F. J., Joubert, F. and Balaban, R. S. (2003) Metabolic network control of oxidative phosphorylation: multiple roles of inorganic phosphate. J. Biol. Chem. **278**, 39155–39165
17 Fujimoto, S., Ishida, H., Kato, S., Okamoto, Y., Tsuji, K., Mizuno, N., Ueda, S., Mukai, E. and Seino, Y. (1998) The novel insulinotropic mechanism of pimobendan: direct enhancement of the exocytotic process of insulin secretory granules by increased Ca^{2+} sensitivity in β-cells. Endocrinology **139**, 1133–1140
18 Takehiro, M., Fujimoto, S., Shimodahira, M., Shimono, D., Mukai, E., Nabe, K., Radu, R. G., Kominato, R., Aramaki, Y., Seino, Y. and Yamada, Y. (2005) Chronic exposure to β-hydroxybutyrate inhibits glucose-induced insulin release from pancreatic islets by decreasing NADH contents. Am. J. Physiol. **288**, E372–E380
19 Schultz, V., Sussman, I., Bokvist, K. and Tornheim, K. (1993) Bioluminometric assay of ADP and ATP at high ATP/ADP ratios: assay of ADP after enzymatic removal of ATP. Anal. Biochem. **215**, 302–304
20 Votyakova, T. V. and Reynolds, I. J. (2001) $\Delta\psi_m$-Dependent and -independent production of reactive oxygen species by rat brain mitochondria. J. Neurochem. **79**, 266–277
21 Leung, A. W., Varanyuwatana, P. and Halestrap, A. P. (2008) The mitochondrial phosphate carrier interacts with cyclophilin D and may play a key role in the permeability transition. J. Biol. Chem. **283**, 26312–26323
22 Detimary, P., Gilon, P., Nenquin, M. and Henquin, J. C. (1994) Two sites of glucose control of insulin release with distinct dependence on the energy state in pancreatic B-cells. Biochem. J. **297**, 455–461
23 Detimary, P., Van den Berghe, G. and Henquin, J. C. (1996) Concentration dependence and time course of the effects of glucose on adenine and guanine nucleotides in mouse pancreatic islets. J. Biol. Chem. **271**, 20559–20565
24 Detimary, P., Gilon, P. and Henquin, J. C. (1998) Interplay between cytoplasmic Ca^{2+} and the ATP/ADP ratio: a feedback control mechanism in mouse pancreatic islets. Biochem. J. **333**, 269–274
25 Katz, L. A., Swain, J. A., Portman, M. A. and Balaban, R. S. (1988) Intracellular pH and inorganic phosphate content of heart *in vivo*: a ^{31}P-NMR study. Am. J. Physiol. **255**, H189–H196
26 Katz, L. A., Swain, J. A., Portman, M. A. and Balaban, R. S. (1989) Relation between phosphate metabolites and oxygen consumption of heart *in vivo*. Am. J. Physiol. **256**, H265–H274
27 Bunger, R., Mallet, R. T. and Hartman, D. A. (1989) Pyruvate-enhanced phosphorylation potential and inotropism in normoxic and postischemic isolated working heart. Near-complete prevention of reperfusion contractile failure. Eur. J. Biochem. **180**, 221–233
28 Ghosh, A., Ronner, P., Cheong, E., Khalid, P. and Matschinsky, F. M. (1991) The role of ATP and free ADP in metabolic coupling during fuel-stimulated insulin release from islet beta-cells in the isolated perfused rat pancreas. J. Biol. Chem. **266**, 22887–22892
29 Erecińska, M., Bryła, J., Michalik, M., Meglasson, M. D. and Nelson, D. (1992) Energy metabolism in islets of Langerhans. Biochim. Biophys. Acta **1101**, 273–295
30 Palmieri, F., Prezioso, G., Quagliariello, E. and Klingenberg, M. (1971) Kinetic study of the dicarboxylate carrier in rat liver mitochondria. Eur. J. Biochem. **22**, 66–74
31 Crompton, M., Palmieri, F., Capano, M. and Quagliariello, E. (1974) The transport of sulphate and sulphite in rat liver mitochondria. Biochem. J. **142**, 127–137
32 Brown, G. C., Lakin-Thomas, P. L. and Brand, M. D. (1990) Control of respiration and oxidative phosphorylation in isolated rat liver cells. Eur. J. Biochem. **192**, 355–362
33 Valdez, L. B., Zaobornyj, T. and Boveris, A. (2006) Mitochondrial metabolic states and membrane potential modulate mtNOS activity. Biochim. Biophys. Acta **1757**, 166–172
34 Dzbek, J. and Korzeniewski, B. (2008) Control over the contribution of the mitochondrial membrane potential ($\Delta\psi$) and proton gradient (ΔpH) to the protonmotive force (Δp). *In silico* studies. J. Biol. Chem. **283**, 33232–33239
35 Martin, D. B. (1995) Bioenergetics. In A Practical Approach (Brown, G. C. and Cooper, C. E., eds), pp. 39–62, Oxford University Press, Oxford
36 Oliveira, G. A. and Kowaltowski, A. J. (2004) Phosphate increases mitochondrial reactive oxygen species release. Free Radic. Res. **38**, 1113–1118
37 Kunz, W., Gellerich, F. N., Schild, L. and Schönfeld, P. (1988) Kinetic limitations in the overall reaction of mitochondrial oxidative phosphorylation accounting for flux-dependent changes in the apparent $\Delta G^{ex}_P/\Delta\mu H^+$ ratio. FEBS Lett. **233**, 17–21
38 Nicholls, D. G. (1974) The influence of respiration and ATP hydrolysis on the proton-electrochemical gradient across the inner membrane of rat-liver mitochondria as determined by ion distribution. Eur. J. Biochem. **50**, 305–315
39 Duszyński, J., Bogucka, K. and Wojtczak, L. (1984) Homeostasis of the protonmotive force in phosphorylating mitochondria. Biochim. Biophys. Acta **767**, 540–547

40 Ouhabi, R., Rigoulet, M., Lavie, J. L. and Guérin, B. (1991) Respiration in non-phosphorylating yeast mitochondria. Roles of non-ohmic proton conductance and intrinsic uncoupling. Biochim. Biophys. Acta **1060**, 293–298
41 Czyż, A., Szewczyk, A., Nałcz, M. J. and Wojtczak, L. (1995) The role of mitochondrial potassium fluxes in controlling the protonmotive force in energized mitochondria. Biochem. Biophys. Res. Commun. **210**, 98–104
42 Rigoulet, M., Fraisse, L., Ouhabi, R., Guerin, B., Fontaine, E. and Leverve, X. (1990) Flux-dependent increase in the stoichiometry of charge translocation by mitochondrial ATPase/ATP synthase induced by almitrine. Biochim. Biophys. Acta **1018**, 91–97
43 Hafner, R. P., Brown, G. C. and Brand, M. D. (1990) Analysis of the control of respiration rate, phosphorylation rate, proton leak rate and protonmotive force in isolated mitochondria using the 'top-down' approach of metabolic control theory. Eur. J. Biochem. **188**, 313–319
44 Lambert, A. J. and Brand, M. D. (2004) Superoxide production by NADH:ubiquinone oxidoreductase (complex I) depends on the pH gradient across the mitochondrial inner membrane. Biochem. J. **382**, 511–517
45 Nobes, C. D., Brown, G. C., Olive, P. N. and Brand, M. D. (1990) Non-ohmic proton conductance of the mitochondrial inner membrane in hepatocytes. J. Biol. Chem. **265**, 12903–12909

Received 19 October 2010/21 January 2011; accepted 25 January 2011
Published as BJ Immediate Publication 25 January 2011, doi:10.1042/BJ20101708

Transplant International

Transplant International ISSN 0934-0874

ORIGINAL ARTICLE

Three-dimensional *ex vivo* imaging and analysis of intraportal islet transplants

Hiroyuki Fujimoto,[1] Kentaro Toyoda,[1] Teru Okitsu,[2] Xibao Liu,[1,2] Eri Mukai,[1] Xiaotong Zhuang,[1] Shinji Uemoto,[3] Naoki Mochizuki[4] and Nobuya Inagaki[1,5]

1 Department of Diabetes and Clinical Nutrition, Graduate School of Medicine, Kyoto University, Kyoto, Japan
2 Transplantation Unit, Kyoto University Hospital, Kyoto, Japan
3 Division of Hepato-Pancreato-Biliary Surgery and Transplantation, Department of Surgery, Graduate School of Medicine, Kyoto University, Kyoto, Japan
4 Department of Cell Biology, National Cerebral and Cardiovascular Center Research Institute, Osaka, Japan
5 CREST of Japan Science and Technology Cooperation (JST), Kyoto, Japan

Keywords
allogeneic transplantation, islet transplantation, optical projection tomography, syngeneic transplantation, three-dimensional images.

Correspondence
Nobuya Inagaki, 54 Shogoin Kawahara-cho, Sakyo-ku, Kyoto 606-8507, Japan. Tel.: +81-75-751-3560; fax: +81-75-751-4244; e-mail: inagaki@metab.kuhp.kyoto-u.ac.jp

Conflicts of Interest
All authors have no conflict of interest.

Received: 13 December 2010
Revision requested: 17 January 2011
Accepted: 21 April 2011
Published online: 25 May 2011

doi:10.1111/j.1432-2277.2011.01271.x

Summary

In clinical islet transplantation, because the long-term insulin-independence rate is still poor, a method for detailed analysis of the transplanted islets in the liver after transplantation is required. We have established a novel imaging technique suitable for analysis of transplanted islets in liver using an optical projection tomography (OPT) method. A three-dimensional tomographic image of the transplanted islets in liver was reconstructed. The number of islets transplanted and the number of transplanted islets observed using OPT showed good correlation. The OPT method was used to compare the numbers of transplanted islets in mouse syngeneic and allogeneic transplantation models. Blood glucose concentrations of streptozotocin (STZ)-induced diabetic mice transplanted with syngeneic islets remained normoglycemic and the number of transplanted islets was largely preserved 11 days after transplantation. In mice transplanted with allogeneic islets, hyperglycemia recurred from 7 days after transplantation and the number and the volume of transplanted islets was significantly reduced 11 days after transplantation. These results indicate that OPT imaging and analysis may be a useful tool to quantitatively and sterically evaluation of transplanted islets in liver at the cellular level.

Introduction

Islet transplantation is a promising therapeutic approach for patients with insulin-dependent diabetes mellitus to achieve insulin independence [1,2]. A remarkably high rate of freedom from insulin therapy is achieved in insulin-dependent type 1 diabetic patients after islet transplantation by the Edmonton Protocol [1]. However, it was reported that long-term maintenance of glucose homeostasis without the use of insulin is poor [3]. This decline may be attributed to progressive islet loss as well as to various reactions during and after islet transplantation, including mechanical injury, ischemia, and nonspecific inflammatory reactions [4].

Until now, the total functional volume of islets transplanted intraportally in liver could be monitored only indirectly by measurements such as blood glucose and serum c-peptide levels. Modalities including bioluminescence imaging (BLI) [5–7], magnetic resonance imaging (MRI) [8–11], and positron emission tomography (PET) [12–14] have been used, and transplanted islets were detected by MRI [11] and PET [13] in human. These methods are suitable for *in vivo* examination because they are noninvasive and can be repeated over time. However, islets cannot be evaluated at the cellular level by these methods because the resolution is too low. Conventional immunohistochemical method permit evaluation of beta-cell volume at the subcellular level, but

can only restricted, sliced areas of the sample can be observes. Recently, Hara *et al.* reported subcellular analysis of intact pancreas, but the method can analyze only thin neonatal samples [15]. To investigate engraftment of transplanted islets scattered in solid liver at the subcellular level, another method is required. We have demonstrated an optical projection tomography (OPT) technique for precisely, three-dimensionally evaluating transplanted islets at the cellular level in liver.

Optical projection tomography is a microscopic imaging technique for obtaining three-dimensional, reconstructed images of small biological samples [16]. The principle of OPT is that the light passes through the specimen labeled and cleared for a standard back-projection algorithm to generate a relatively high resolution tomographic image. A three-dimensional image of the specimen is reconstructed using the individual tomographic images. The advantage of OPT is the capability to investigate spatial distribution of such target molecules as RNA and protein without slicing of the target organs and at a higher resolution.

In this report, we show that the number and volume of intraportally transplanted islets in liver can be investigated using OPT analysis. In addition, comparing syngeneic and allogeneic rodent islet transplantation models, we demonstrate that the number and volume of transplanted islets is considerably more decreased in allogeneic islet transplantation than in syngeneic transplantation. Thus, *ex vivo* imaging of intraportal islet transplant using OPT may be a useful tool for evaluation and improvement of islet transplantation outcome.

Materials and methods

Animals

Male C57BL6 Cr Slc mice (Shimizu Laboratory Supplies Co. Ltd, Kyoto, Japan) aged 8–10 weeks were used as recipients and donors and male BALB/c mice (Shimizu Laboratory Supplies Co. Ltd) aged 8 weeks were used as recipients for allogeneic transplantation. All experiments were approved by the Kyoto University Animal Care Committee.

Islet isolation and islet transplantation

Islets were isolated from mouse pancreas using collagenase digestion method [17]; 3–4 ml Hank's Balanced Salt Solution (HBSS) containing 0.5 mg/ml collagenase (Nitta Gelatin, Osaka, Japan) was infused through the common bile duct. The pancreas was dissected and digested at 37 °C for 21 min. Islets were separated from exocrine cells by centrifugation with Ficoll-Conray gradient solution for 10 min. Diabetes was rendered by a single intraperitoneal injection of streptozotocin (STZ) (Nacalai Tesque, Kyoto, Japan), 120 mg/kg body weight, freshly dissolved in 10 mM citrate buffer (pH 4.5). These mice were used as diabetic recipients if the blood glucose concentration was more than 20 mM on two consecutive days. Recipient mice were anesthetized by isoflurane (Forane; Abott, Chicago, IL, USA) during transplantation. Fresh islets in a volume of about 400 μl HBSS were injected into the portal vein and transplanted into the right hepatic lobe as previously reported [18]. For validation of the OPT method, 75, 150 or 300 islets were transplanted into the right hepatic lobe, which was dissected immediately after transplantation. For comparison of syngeneic and allogeneic transplantation, C57BL6 mice (H-2^b) were used as recipients; 300 islets isolated from C57BL6 mice or Balb/c mice (H-2^d) were transplanted, respectively. The blood glucose concentration was determined by glucose meter (Glucocard, Arkley, Japan).

Tissue preparation and immunostaining

Mice with transplanted islets were sacrificed by cervical dislocation. The transplanted right hepatic lobes were dissected clean and immediately immersed for fixation in 4% paraformaldehyde in PBS for 3 h at 4 °C. The fixed samples were washed in PBS and then transferred stepwise to 100% methanol (MeOH) and stored at −20 °C. The immunostaining was performed according to the previous report [19] as follows. The right hepatic lobe was immersed in 15% H_2O_2, 16.7% DMSO solution in MeOH for 24 h to bleach pigmented cells and to reduce auto fluorescence. The liver then was washed in MeOH, which was repeated five times and then kept at −80 °C for at least 1 h before return to room temperature. The organ was rehydrated by Tris Buffered Saline-TritonX (TBST) [0.15 M NaCl (Nacalai Tesque, Kyoto, Japan), 0.1 M Tris (hydroxymethy)aminomethane (Nacalai Tesque, Kyoto, Japan) pH 7.4, and 0.1% Triton X-100 (Nacalai Tesque, Kyoto, Japan)]. TBST containing 10% normal goat serum (Dako Corp., Glostrup, Denmark) and 0.01% sodium azide (Nacalai Tesque, Kyoto, Japan) was used as blocking solution for 24 h. The organ was incubated in insulin antibody (Santa Cruz Biotechnology Inc., Santa Cruz, CA, USA) in 5% DMSO containing blocking solution for 48 h. After washing, Alexa594 goat anti rabbit IgG (Invitrogen, Carlsbad, CA, USA) was used as secondary antibody for 48 h.

Optical projection tomography and image reconstruction

For the observations, the immunostained liver was embedded in 1% agarose gel (low melting point agarose; Sigma Aldrich, St. Louis, MO, USA) to fix the sample.

OPT was performed using an OPT scanner (OPT scanner 3001; Bioptonics, Scotland, UK) according to the manufacturer's instructions [16,19]. The specimens were maintained within the BABB (benzyl alochol/benzyl benzoate 1:2 ratio), rotated to a series of angular positions (0.9° apart) and images were captured at each orientation. High-resolutional tomographic images were reconstructed from raw images by NRecon software (SKYSCAN, Kontich, Belgium). The tomographic images obtained from OPT were reconstructed to three-dimensional form and analyzed by Avizo software (Visualization Science Group, Inc., Burlington, MA, USA). Three-dimensional images of islets and liver were obtained by isosurface treatment. Total volume of all islets was calculated by summation of the selected islets.

Statistical analysis

Data and graph were presented as medians (interquartile range) and statistical analysis was performed with Mann–Whitney's *U*-test. A value of $P < 0.05$ was considered significant.

Results

Observation of transplanted islets in liver by OPT

Transparency of the liver and immunostaining of transplanted islets without sectioning were achieved by the preparation protocols. Figure 1a is a raw OPT image of liver; the insulin-stained transplanted islets are seen as dots in the high magnification image (Fig. 1b, white arrows). One of the tomographic images obtained is shown in Fig. 1c. Vertically reconstructed images are shown in Fig. 1d and e and islets pointed out by arrow and arrowhead in Fig. 1c are located as in Fig. 1d and e, respectively. Some islets appear to be located at the terminal end of the portal vein (Fig. 1c and d) and other islets are located at the wall of the proximal branch of the portal vein (Fig. 1e). Figure 1f is the reconstructed target-specific image of an islet (arrowhead in Fig. 1e) and portal vein. Thus, a three-dimensional image as well as the size and location of transplanted islets in liver can be investigated (Fig. 1g and h and Supplementary movie).

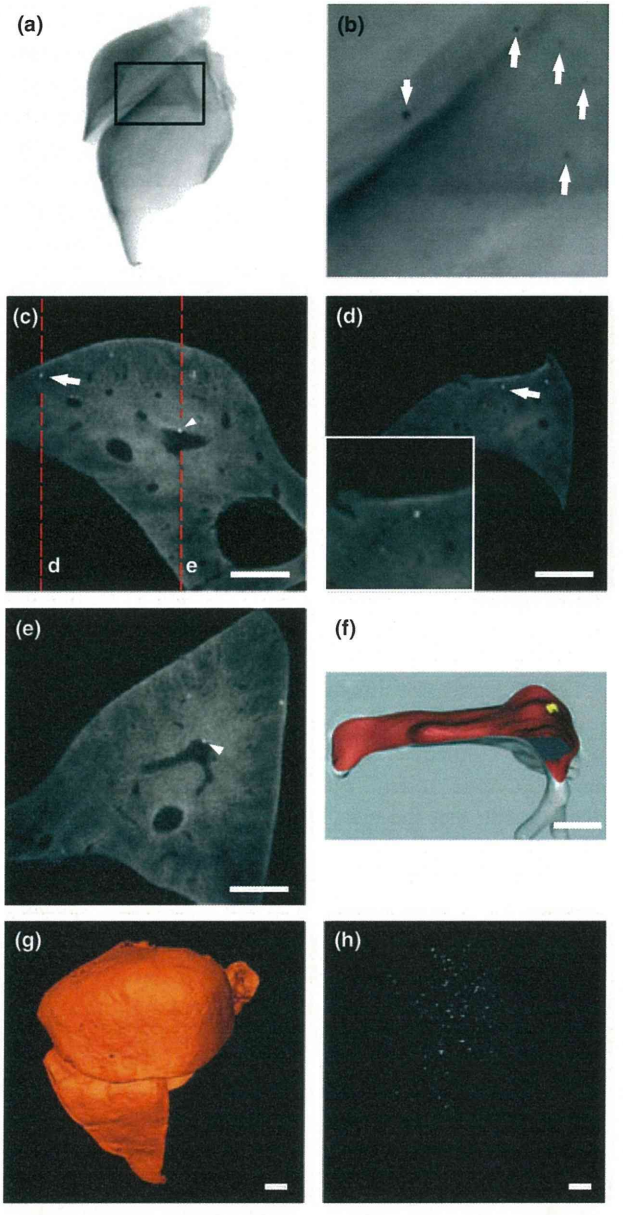

Figure 1 Optical projection tomography (OPT) images of liver containing intraportally transplanted islets. (a) Raw image of islet-transplanted right hepatic lobe, (b) high magnification image [in square of (a)], (c) representative slice image of the transplanted right hepatic lobe; (d and e) vertical slice image of islet with arrow in (c), arrowhead in (c), respectively. (f) Reconstructed three-dimensional image of islet [in (c) and (e), arrowhead] and portal branch. Three-dimensional image of (g) right hepatic lobe; (h) islets (white spots) in liver reconstructed from the same liver sample as (a). Scale bars indicate 1 mm in (c, d, e, g, and h) and 300 μm in (f).

Evaluation of the effectiveness of OPT analysis of transplanted islets in liver

To correlate the number of islets transplanted and the number of islets detected by OPT, we resected and fixed livers immediately after transplantation of a range of numbers of islets. The three-dimensional reconstructed image shows that the number of spots indicating transplanted islets in the right hepatic lobes was increased in accord with the increased dosage (Fig. 2a–c); these numbers are well correlated ($r^2 = 0.9561$) (Fig. 2d). These findings indicate that OPT can be used for quantitative analysis of islets transplanted into liver.

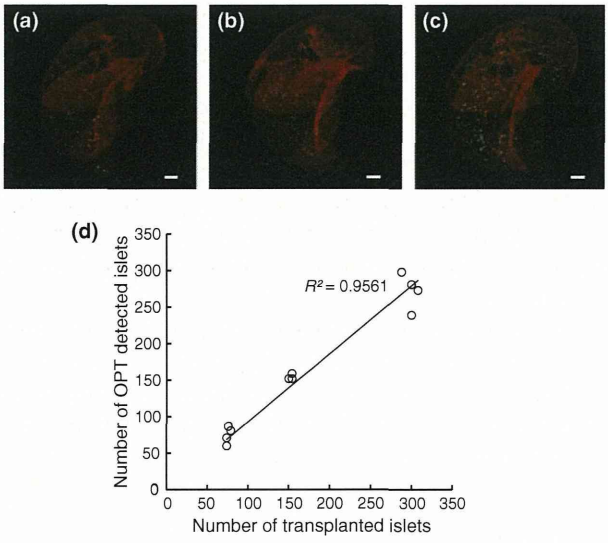

Figure 2 Comparison of the number of islets transplanted with that obtained by optical projection tomography (OPT) analysis. Representative OPT image of recipient liver transplanted with (a) 75, (b) 150, and (c) 300 islets, respectively. (d) Correlation of the number of islets transplanted and OPT-detected islets. Scale bar indicates 1 mm.

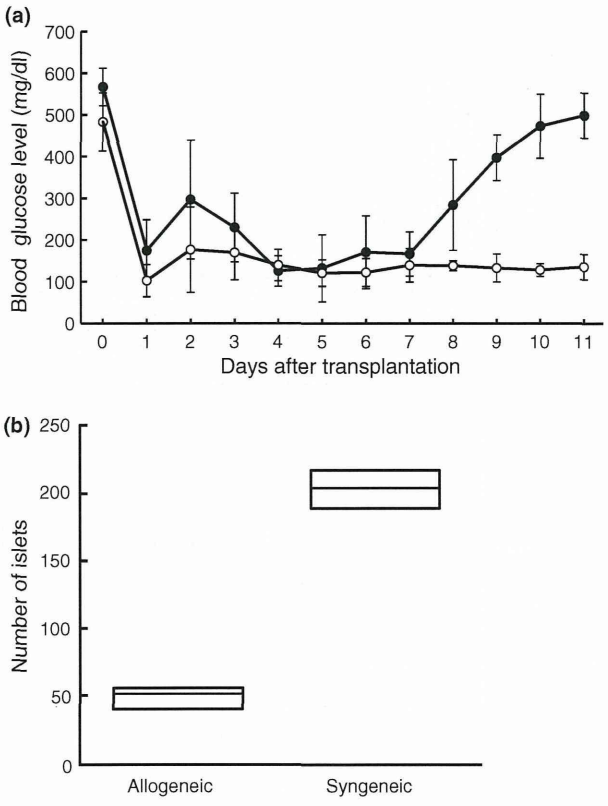

Figure 3 Glycemic level and number of islets of streptozotocin (STZ)-induced diabetic mice after syngeneic and allogeneic islet transplantation. (a) Random blood glucose level of recipients (open circles: syngeneic transplantation, filled circles: allogeneic transplantation). (b) Number of transplanted islets in syngeneic and allogeneic transplantation 11 days after transplantation.

Optical projection tomography analysis of islet grafts under syngeneic and allogeneic conditions

To evaluate the time course of transplanted islets in syngeneic and allogeneic conditions, we analyzed the number and volume of islets intraportally transplanted in liver of STZ-induced diabetic mice. Blood glucose concentrations under both syngeneic and allogeneic conditions were normoglycemic until a week after transplantation. However, blood glucose concentrations under allogeneic conditions thereafter became hyperglycemic, while those under syngeneic conditions remained normoglycemic (Fig. 3a). The islet-containing livers were resected on day 11 for analysis using OPT method. The number of islets in the syngeneic condition was dramatically greater than that in the allogeneic condition [52 (IQR 16.5) vs. 203 (28.5), respectively, $P < 0.05$] (Fig. 3b).

In OPT-detected islets classified by size, the number in each category was significantly greater in syngeneic than in allogeneic conditions and showed a similar histogram pattern (Fig. 4a). Total volume of islets in syngeneic condition was dramatically greater than that in allogeneic condition [8.6 (2.7) vs. 35.3 (10.1) ($\mu m^3 \times 10^6$)], respectively, ($P < 0.05$) (Fig. 4b).

Discussion

In this study, we demonstrate that islets transplanted intraportally in liver can be analyzed at the cellular level using OPT method, which permits three-dimensional analysis of the distribution of the islets in the liver. Comparing syngeneic and allogeneic islet transplantation models, we show by OPT that the volume of transplanted islets differs significantly at the cellular level.

One of main problems in clinical islet transplantation, poor long-term achievement of insulin independence, is primarily attributed to graft loss caused by various stressors upon transplantation [4]. When islets are injected intraportally, each of them is thought to locate at the respective branched end of the portal vein in liver. In modalities such as BLI, MRI, and PET, only PET allows quantification of graft volume, but the resolution is still too low for detailed analysis of the transplanted islets. On the other hand, while the resolution of conventional immunohistochemistry is high, only restricted slices of the engrafted organ can be analyzed using this method.

Optical projection tomography, a newly developed method, is reported to permit analysis of a sample at resolution as high as 5 μm. Recently, Alanentalo *et al.* performed detailed analysis of NOD mice during progression